Hoffman / ELECTRONICS CORPORATION
Semiconductor Division
Hoffman Electronic Park, El Monte, California 91734 • 686-0123

Final Report

for

INTEGRAL GLASS COATINGS FOR SOLAR CELLS

(4 May 1964 - 4 Nov. 1964)

Contract No. NAS 5-3857

Prepared by

Hoffman Electronics Corporation
Semiconductor Division
El Monte, California

GPO PRICE $

OTS PRICE(S) $

Hard copy (HC) $3.00

Microfiche (MF) $0.75

For

Goddard Space Flight Center

Greenbelt, Maryland

FACILITY FORM 602

N65-21322 (ACCESSION NUMBER)

91 (PAGES)

CR-57963 (NASA CR OR TMX OR AD NUMBER)

1 (THRU)

(CODE)

03 (CATEGORY)

Hoffman

Rqt 27417

Final Report

for

INTEGRAL GLASS COATINGS FOR SOLAR CELLS

(4 May 1964 - 4 Nov. 1964)

Contract No. NAS 5-3857

Prepared by

Hoffman Electronics Corporation
Semiconductor Division
El Monte, California

For

Goddard Space Flight Center
Greenbelt, Maryland

Report Prepared By: Peter A. Iles
Project Leader

ABSTRACT

21322

This report describes a research program investigating integral glass coatings for solar cells. The technology used and the results obtained are given in detail.

Cells with conversion efficiencies up to 10%, in air mass zero solar illumination, were made in development quantities. The glass layer thickness could be varied from 2 microns to 20 mils. The methods developed show considerable promise, particularly for space missions where very light weight passive thermal control is required, and where the radiation environment consists mainly of low energy particles. The feasibility of coating production quantities of cells has been demonstrated.

Author

TABLE OF CONTENTS

		Page
1.	INTRODUCTION	1
2.	PARTICULAR PROBLEMS OF SOLAR CELLS IN SPACE	1
	2.1 Thermal Control	1
	2.2 Micrometeorite Erosion	1
	2.3 Radiation Effects	2
3.	SOLUTIONS TO SPACE PROBLEMS	3
	3.1 Thermal Control	3
	3.2 Micrometeorite Protection	4
	3.3 Minimizing Deterioration from Radiation	4
	3.4 Methods for Holding Covers	4
	3.5 Discussion of Adhesive - Cover System	5
	3.6 Reasons for Integral Coatings	6
4.	PRESENT PRACTICAL TECHNIQUES	7
	4.1 Choice of Glass	7
	4.2 Slurry Formation and Control	8
	4.3 Fusing Conditions	9
	4.4 Solar Cell Processing Methods	10
	4.5 Comparison of Methods	11
	4.6 Design of Contacts Compatible with the Fusing Cycle	11
5.	MEASUREMENTS AND RESULTS	13
	5.1 Glass Thickness - Measurement and Control	13
	5.2 Topography and Imperfections	15
	5.3 Thermal Emittance Results	28
	5.4 Solar Cell Characteristics	33
	5.5 Measured Results on Cells and Contacts	39
	5.6 Particle Irradiation	50
	5.7 State of Art Samples	63

TABLE OF CONTENTS (CONTINUED)

	Page
6. ASSOCIATED TOPICS	68
7. SURVEY OF CONTRACT, AND CONCLUSIONS	71
8. NEW TECHNOLOGY	74
9. REFERENCES	75
APPENDIX I. Total Hemispherical Emittance Measurements	I-1

LIST OF ILLUSTRATIONS

Figure No.	Caption	Page
1	Thickness Measurement by Differential Focusing Method	14
2	Relative Transmittance of Slurries as a Function of Wavelength	16
3	Relative Transmittance Measurements as a Function of Time	17
4	Layer Thickness as a Function of Slurry Transmittance	18
5a	Actual Density Versus Relative Transmittance	19
5b	Layer Thickness Versus Actual Density	19
6	Photograph Showing Glass Layer Fill-in	20
7	Photograph Showing Glass Layer Fill-in	21
8	Interference Photographs of Glass Surfaces	23
9	Interference Photographs of Good Glass Surfaces	24
10	Photographs of Cleaved Section of Silicon Slice with Glass Layer	25
11	Photographs Showing Transparency of Fused Glass	26
12	Total Hemispherical Emittance as a Function of Temperature	30
13	Total Hemispherical Emittance as a Function of Temperature	31
14	Emittance at 30°C as a Function of Glass Thickness	32
15	Solar Cell Photovoltaic I-V Curve	34
16	Typical Solar Cell Configuration	36

LIST OF ILLUSTRATIONS (CONTINUED)

Figure No.	Caption	Page
17	Relative Spectral Response	38
18	I_{SC} as a Function of Built Up Thickness of Fused Layers	41
19	I-V Curves for Various Fusing Temperatures	45
20	Contact Resistance Versus Number of Heating Cycles	51
21	Transmission Versus Wavelength for Various Slides	55
22	I_{SC} Values for Radiation Batches, Before and After Irradiation	56
23	Typical Spectral Response Curves	59
24	I-V Curves for Batch R10	60
25	I-V Curves for Batch R13	61
26	I-V Curves for Batch R2	62
27	I-V Curves for State of the Art Samples	65
28	Thickness of Glass Layers on 10 State of Art Samples	66
29	Photograph of Solar Cell Partly Covered with Integral Glass	67
I-1	Views of Emittance Sample and Equipment	I-2
I-2	Power Loss Versus Pressure as a Function of Temperature Difference Between Sample and Surroundings	I-4

LIST OF TABLES

Table No.	Caption	Page
1	Effects of Cell Covers on $\frac{\alpha}{\epsilon}$ Ratio, and on Cell Output	3
2	Details of Emittance Samples Used	29
3	Separate Effects of Heat Treatment and Glass Fusion	44
4	Particle Irradiation Samples	53
5	Values of I_{SC} Before and After Electron Irradiation	54
6	Values of Relative Response at Two Wavelengths for Radiation Batches	58
I-1	Raw Data for Emittance Measurements	I-6
I-2	Equilibrium Temperature for Emittance Measurements	I-7

INTEGRAL GLASS COATINGS FOR SOLAR CELLS

1. INTRODUCTION

On satellite missions of fairly long duration, secondary power for gathering or sending information has generally been supplied by solar cell supplies. Typical present-day supplies use several thousand silicon solar cells, of closely controlled and matched characteristics, each cell with a conversion efficiency, measured under equivalent space sunlight, of above 11%. The cells are attached to a light strong substrate, such as aluminum honeycomb, bearing printed circuit contacts which interconnect the solar cells in series and parallel, with pick off points to supply the various power needs. Chemical batteries recharged by the solar cells, provide power storage. This combination has proved reliable under the stresses of launching and of continued operation in the space environment.

2. PARTICULAR PROBLEMS OF SOLAR CELLS IN SPACE

Three problems are particular to the space environment, and are discussed now in turn.

2.1 Thermal Control

Since the only heat loss in space is by radiation, the equilibrium temperature of the satellite is determined by the overall ratio of absorptivity (α) to emissivity (ϵ) of the satellite surface. In the cases where much of this surface is covered with solar cells, the properties of the cell surfaces have a large influence on the satellite temperature. Also because cell output decreases as the temperature increases, the cell $\frac{\alpha}{\epsilon}$ ratio should be as low as possible.

2.2 Micrometeorite Erosion

Micrometeorites striking the space craft erode or remove thin layers of the satellite outer surface. This could degrade a thin coating used for passive temperature control. Also solar cells are very susceptible to such impacts, both because

of their thin antireflecting coating, and also because the PN junction responsible for the energy conversion, is very shallow in cells optimized for high output in space.

2.3 Radiation Effects

The space solar spectrum is rich in ultraviolet radiation, and also there may be large fluxes of electrons and/or protons, particularly in the radiation belts surrounding the earth. Both uncharged and charged radiation can affect dielectric properties, and in addition the particles can produce damage in the semiconductor used in the solar cells, and thereby reduce cell output.

3. SOLUTIONS TO SPACE PROBLEMS

The problems described in Section 2 have been mainly solved. The solutions are given in the next three sections, and are discussed in the later sections.

3.1 Thermal Control

The thermal emittance of silicon is low, and the best way to decrease the $\frac{\alpha}{\epsilon}$ ratio is to cover the cells with a highly emitting, optically transparent cover such as glass or quartz. Typical calculations of the improved temperature control are summarized in Table 1, taken from reference 1. The assumptions made to calculate these figures were that the solar intensity was 140 mW/cm^2, incident normally on cells, oriented to face the sun, with the emissivity of the back of the substrate = 0.9. The results quoted are for a P/N cell of 10% efficiency at 28°C, but will be similar for an 11% N/P cell. Bare cells (case 1) are seen to run at 85°C, and they cool to 46°C when a glass cover is added (case 2). Generally these covers are bonded to the cell by a thin layer of transparent adhesive. However, since most adhesives darken under the enhanced ultraviolet radiation, the reliability of the cell plus cover combination is increased by applying an ultraviolet rejection filter of many (up to 18) alternate dielectric layers evaporated with carefully controlled thicknesses. This gives case 3, where the penalty for the added reliability

TABLE 1. Effects of cell covers on $\frac{\alpha}{\epsilon}$ ratio, and on cell output.

	Case	$\frac{\alpha}{\epsilon}$	In-Space Temperature	Loss From 28°C Output	Net Gain Of[+] Output Over Bare Cell
1.	Bare P/N cell	2.5	85°C	23%	--
2.	P/N cell + glass* cover	0.97	46°C	8%	16%
3.	P/N cell + glass* cover with UV rejection filter	0.97	46°C	8%	8.5%
4.	P/N cell + glass* cover with UV and IR rejection filters	0.84	35°C	4%	11%

+ The net gain includes transmission losses in the coatings.

*glass - 6 mil Corning 0211 glass with antireflecting coating.

is the lower net gain. Some restoration of output (case 4) is gained by adding to the side of the cover in contact with the adhesive, another filter rejecting some infrared radiation, of wavelength greater than 1.2 microns. This rejected radiation does not form hole electron pairs because it is less energetic than the energy gap of silicon.

3.2 Micrometeorite Protection

The covers used for thermal control can also protect against large scale deterioration from micrometeorites. Experience has shown that the frequency of impacts is lower than predicted. The worst case is expected when the transparent cover becomes severely abraded, causing around 20% loss in transmission, but no reduction in temperature control or of other cell properties.

3.3 Minimizing Deterioration From Radiation

Two methods have been used to reduce cell degradation from radiation damage. First the cell itself can be made less sensitive by using the N/P structure (reference 2) and then further by reducing the acceptor impurity concentration in the bulk silicon, or by selecting the optimum dopant (aluminum instead of boron) (reference 3). Increased radiation resistance can result from including a drift field in the bulk of the cell, but at present such cells are not available in production quantities with performance or costs comparable to conventional cells. The second way to add radiation resistance is to use transparent shields. The thickness needed varies according to the density and energy of the particles encountered. Covers as thick as 60 mils of quartz have been used, but for many orbits, particularly those well clear of the earth, covers of glass 3 mils thick provide adequate protection (reference 4).

3.4 Methods For Holding Covers

By suitable choice of the thickness and nature of the transparent covers, solar cells have coped well with the above problems for the operating conditions in many different orbits. Historically, three methods have been used to hold the covers over the cells: Earliest satellites (eg. Vanguard I)

used thick (65 mils) quartz covers held on the cells with a housing and a gasket seal. These covers were used before radiation damage was expected, and were intended mainly for micrometeorite protection. However, the relatively large shield thickness has allowed continued operation of the solar cells. The second method, most commonly used, relied on adhesive bonding. The adhesive systems presently used are elastomeric in nature and have good transmission over the spectral range where the cells are sensitive. By these means, thin (6 mil) glass slides for temperature control, and later thick (up to 60 mils) quartz slices for additional radiation protection have been bonded to the cell surfaces. Lastly, the Telstar power supplies (reference 5) eliminated the adhesive, and used a 30 mil sapphire cover fused to platinum supports. This method is more complex and expensive than the other methods.

3.5 Discussion Of Adhesive-Cover System

The advantages and disadvantages of the second method (adhesive bonding) can be given:

a) Advantages

i) The system is well proven in many space missions.

ii) Since only low temperatures are needed for curing the adhesive, and the cover has good optical transparency, the high output of the bare cell can be retained. The degradation of short circuit current caused by the applied cover can be as low as 2% for glass covers, and 5% for thick quartz covers.

iii) Good cell temperature control has been achieved.

iv) The system is versatile, providing a wide range of radiation protection (governed by weight restrictions of specific missions). A large amount of mismatch between cells and covers can be accommodated.

v) Covers can be applied to already connected modules since the adhesive is cured below 150°C.

b) Disadvantages

i) The system is costly, present estimates for 2 cm^2 covers varying from \$0.50 to \$3.50 depending on the covers and filters required. When assembly costs are included, the cover costs can predominate in the completed solar array.

ii) Despite much effort in adhesive selection, the adhesive sets the limit on mechanical strength and on environmental performance, particularly on the possibility of high temperature storage or operation. Also Campbell (Ref. 6) showed that under irradiation, adhesive degradation was sometimes predominant.

iii) The covers, especially those of thin glass are fragile and this complicates array assembly. The fragility adds much difficulty in providing covers thinner than 6 mils. For some missions, such thinner covers are sufficient and are of advantage in reducing the weight of the power supply.

3.6 Reasons For Integral Coatings

Integral coatings offer the chance of offsetting the above disadvantages. The work reported here provided quantitative estimates of the effects of removing the need for adhesives, by bonding glass integrally to the solar cell surface.

Before describing the methods used during this work, some of the earlier unsuccessful attempts to provide suitable integral coatings, are recalled. Mostly these trials involved the growth of silicon dioxide films onto silicon, by thermal oxidation, pyrolytic decomposition of silanes, evaporation or sputtering. These methods generally gave slow layer formation rates, often required very high temperatures, and when the layers were thicker than 2 microns, the severe mismatch led to cracking of the silicon dioxide or the silicon. Layers of organic materials like epoxies or elastomers were successfully applied, but present planning for space missions rules out this type of coating, because of the high chance of ultraviolet and vacuum degradation. Early attempts to fuse powdered borosilicate glasses did not give a layer of good transparency, because, it is now realized, the experimental techniques were inadequate.

4. PRESENT PRACTICAL TECHNIQUES

In this work, fine powdered glass is deposited onto silicon, and fused to form an integral coating. The practical techniques have two aspects, control of the glass layer properties, and fabrication of solar cells.

4.1 Choice Of Glass

As usual in glass technology, the choice of the best glass is a compromise between several requirements, some conflicting. The glass should have a thermal coefficient of expansion well matched to that of silicon over a fairly wide temperature range, should be of as low fusing temperature as possible, with good optical transmission when fused, have high thermal emittance and be stable under irradiation. The easiest requirement to meet is that of high thermal emittance, which is the case for most glasses. At first in this work zinc alumino-borosilicate glasses were used because by change of composition, these glasses could have expansion coefficients for 0°C to 300°C, in the range 38 to 45 x 10^{-7} per °C, with fusing temperatures in the range 640°C - 750°C. However, these glasses were found to have serious disadvantages, particularly in low optical transmission, chemical attack by plating solutions and limited fusing properties. Satisfactory layers thicker than 8 microns were difficult to fuse, and excessive bubbles formed in the glass if the fusing temperature exceeded 750°C by a small amount. These disadvantages, together with the possibility that radiation darkening would be more severe than for simpler glass systems, (see Section 5.6 below), led to re-examination of other glasses. This time, because of better control of the glass technology needed, some borosilicate glasses thermally matched to silicon (Corning glasses 7070, 7720, 7040 and 7740) gave successful results, and had some advantages over the more complex glasses. In particular these glasses had higher optical transmission, their fusing temperature range was less critical, and thicker layers of good quality could be applied. The offsetting disadvantages were that fusing temperatures were higher, and that drying patterns were left. The former disadvantage could be tolerated, and the latter was not considered serious, and could be reduced.

4.2 Slurry Formation And Control

The glass was broken into small pieces and was powdered using either an alumina ball mill, or a ceramic rolling mill. Most of the work here used small batches (20 grams) of glass, and the small ball mill. The method used to prepare suitable slurries was based on an IBM method (reference 7). The fine glass was prevented from coagulating, by dispersing it in isopropyl alcohol, a liquid of high dielectric constant (18). In order to provide some degree of coagulation when the glass was deposited onto silicon, a denser liquid, ethyl acetate, of low dielectric constant (6) was mixed with the alcohol, so that the glass leaving this heavier liquid adhered weakly to the silicon.

Earlier uses of this technique (reference 7) generally required pinhole-free, thin films (1 to 5 microns). In the present work, films 10 microns or greater were preferable, and therefore methods suited to thicker layers were developed.

The glass powder formed by milling had a wide range of particle sizes, and for obtaining thicker layers it was decided not to attempt time-consuming particle size analysis. The more practical approach was to find a rapid way to control the slurry content to provide thicker layers of consistent quality. The method developed was very successful. It was based on the use of a Bausch and Lomb Spectronic 20 Colorimeter, which measures the optical transmission through a standard test tube filled with the solution under test. A movable grating allowed variation of wavelength from 350 to 950 millimicrons but because the wavelength dependence of transmission did not appear sensitive to the particle size distribution, most comparisons were taken near the wavelength giving peak transmission, 750 millimicrons. Typical calibration curves are given below (Section 5.1).

The empirical procedure used was as follows: For each glass, an upper density, which did not form good layers after fusing was determined, and controlled densities below this limit were used. The density was reduced by settling under gravity or by slow centrifuging (300-800 rpm). Experience allowed a rapid estimate of the correct combination of centrifuging and settling which gave the required density. The colorimeter was calibrated by using the slurry liquids only, and with aperture width constant, by adjusting the lamp intensity until the full scale reading (transmission = 100%) was obtained at 750 millimicrons.

A constant, low density slurry was then placed in the optical path and the lamp intensity increased to give the full scale reading again. In practice, for the glasses used, and this calibration system, the usable transmission range was 8 to 50%. With this procedure, good adjustment of slurries was possible (see Section 5.1), and fused layers of consistent quality and predictable thickness were obtained.

Cleaned slices of silicon were placed in a beaker and the slurry was poured over the slices. The beaker was spun in a centrifuge at high speed (3000 rpm for 3 minutes), and the glass powder was thrown onto the silicon. The slices were removed from the beaker carefully, to avoid disturbing the lightly adhering glass layer. The liquids dried quickly leaving a thick matte, white glass layer. This layer was fused as soon as possible. Several slight variations were possible at this stage. To reduce thickness variations, especially at the edges of the slice, a small volume of dense liquid with dielectric constant lower than that of ethyl acetate, eg. trichloroethylene (dielectric constant 3.4) could be injected at the bottom of the beaker before centrifuging. Alternate ways of removing the slurry such as decanting or siphoning, were tried but did not show any advantage. It was found advantageous to take extra care in the cleanliness of the cells and the containers. Also to avoid aging effects, slurries were used as soon as possible after they were made.

4.3 Fusing Conditions

The fusing cycle had to be a compromise. The optical qualities of the fused glass layers were found to improve as the temperature increased, as a result of more complete fusion, until a limit was reached, where defects such as bubbles began to appear in the layers. As mentioned above, borosilicate glasses gave a much wider temperature range (820°C - 950°C) where good fusion was possible. The compensating consideration was that there could be degradation of solar cell performance, by bulk and/or contact deterioration, as the temperature - time cycle became more severe. The atmosphere used during fusion affected the glass layer, and generally an inert gas (nitrogen) was used. At first fusion was done in an open tube furnace using temperatures in the range 750°C to 850°C for times of 5 to 10 minutes. Later a strip heater was used. Various controlled cooling cycles, variations of pull rate through the furnace, or annealing

treatments were tried to improve cell performance, but the best combination of glass layer and cell properties resulted from fast cooling. During this work, cell fabrication methods were developed which minimized the combined effects of possible degradation caused by the rapid cooling. The best fusing cycle found was a rapid heating and cooling (15 seconds total) with a peak temperature between 850°C and 950°C. For the second and later layers, the bond between the already fused glass layer and the powder could be formed at slightly lower temperatures. No separate interfaces were noticed between the successive layers.

4.4 Solar Cell Processing Methods

Three methods were used to fabricate cells with integral glass coatings. These methods are described next, with comments on their limitations following.

a) Glass was fused to a diffused slice, the diffused layer on the back side was sandblasted off, and the slice was masked to leave a grid pattern on the glazed surface. The exposed glass was then etched away using hydrofluoric acid or a mixture of this acid with hydrochloric acid. The etch rate of the glass was approximately 0.25 microns per second, but this rate decreased for thicker layers. Metal contacts were made to the cell, back and front, mostly by electroless plating. The junction was etched clean around the edges, and the contacts were soldered.

b) Before fusion, the glass was removed in the required grid pattern, using either a shadow mask during centrifugal application of the glass powder or by scribing the powder while it was still damp, using a solid probe or a small diameter tube connected to a vacuum line. The glass layer was then fused, and any thin glass remaining in the grid pattern was removed by a short etch in hydrofluoric acid. The rest of the processing followed (a), borosilicate glasses having the added advantage in this method in not being plated by the electroless solutions.

c) In this method, contacts were applied, at least on the front surface of the cell, before the glass powder was applied. After fusing, the back contact could be applied and the junction etched clean. A fuller discussion of suitable contact design is given in the section 4.6.

4.5 Comparison Of Methods

(a) and (b) had the advantage that they allowed higher fusing temperatures and therefore possibly better glass layers. For (c) the highest fusing temperature was set by the melting point of the metals used in the contacts (960°C for silver). For (a) there were difficulties in etching away the glass in thicker glass layers while preventing etchant leakage under the mask, with consequently wider grid lines. Also in (a) and (b), part of the front surface consisted partly of metal, thus decreasing the overall thermal emissivity of the cell. For method (b), successive glass layers could be applied only if good grid re-registration was possible. However, there was no need for a mask during plating. In this latter case, the fluoride ions in solution removed the polished surface formed when the glass fused, leaving a matte finish. This matte surface retained the optical transmission of the shiny layers, had lower reflectivity and had the highest thermal emittance measured in this work. This matte finish could be applied to the glass surface in any of the three methods, by a dip in HF (see Figure 10 for photographs of these surfaces). Method (b) still could not yield very thin grid lines. Method (c) overcame the defects of (a) and (b) so well that a detailed investigation of compatible contacts was undertaken. With adequate contacts, it was possible to get thick layers, covering most of the front surface, all of it if a wraparound contact structure was used. In addition, these contacts added considerable versatility, in that thick cover slides (6 mils and above) made from glass similar to that used in the slurry could be bonded to the cell either by using a layer of fused powder as a "solder", or by direct fusion. In this way, thick integral covers could be provided with only one or two fusing cycles. The reduction in fusing cycles enabled close design of the contact structure.

4.6 Design Of Contacts Compatible With The Fusing Cycle

Present day N/P silicon solar cells have either plated contacts, or use the evaporated and sintered titanium-silver contacts developed by Western Electric (reference 5). For the latter, although the sintering is carried out around 610°C, the glass fusion cycle, caused some penetration of the metals through the shallow diffused layer, with seriously reduced output.

The plated contact degraded by the same mechanism at temperatures as low as 400°C, and in the fusing range there was the additional possibility of severe reduction in bulk minority carrier lifetime because of gold diffusion from the plating.

Originally it was planned to avoid these effects by using a double diffusion method, wherein the front contacts were evaporated over regions with a relatively deep P/N junction (several microns), whereas the rest of the active area of the cell was diffused later to leave a shallow P/N junction (0.3 microns), to provide high output in space sunlight. This method was tried with some success, but the double diffusion and the need for close re-registration of the contact pattern made it a complex method.

In this work, a new method was developed and proved very successful. The principle used was to include a thin dielectric layer between the diffused surface and the evaporated metals. By carefully controlling the thicknesses of the metal and dielectric layers, it could be arranged that during the glass fusion cycle, the metals penetrated to make ohmic contact to the diffused layer, while further penetration of the diffused layer was retarded. The first dielectric layer tried for this purpose was the phosphorosilicate layer left on N/P cells after phosphorus diffusion. Already the thickness of this layer was carefully controlled around 0.3 microns, and it had provided the antireflecting coating on Hoffman N/P cells for three years. By evaporating titanium-silver on top of this coating, a good approach to the contact problem was achieved. Details of cells made using these contacts are given below (Sections 5.5 to 5.7). Also evaporated layers of silicon monoxide of thickness 800, 1600, 2400 and 3200 Å were tried, but although fairly successful, only the 800 Å layer gave good antireflecting properties. These thinner layers were generally less successful than the phosphorosilicate glass in preventing contact penetration.

5. MEASUREMENTS AND RESULTS

This section summarizes the quantitative results which have been obtained on the glass layers, and on the glass coated cells.

5.1 Glass Thickness - Measurement And Control

Measurement

Several ways of measuring the glass layer thickness were available, depending on the thickness. For very thin layers, these involved destructive methods, such as grooving or angle sectioning or interferometric measurement of a step formed by removing some of the glass.

For the thickness range used most in this work (0.5 to 2 mils) a sensitive dial gage could be used, measuring the slice thickness before and after the glass layer was applied. However, for this range the most convenient method, which required no destructive steps used differential focusing of a microscope and is shown schematically in Figure 1. First the refractive index (n) of the glasses was measured, by focusing a microscope in turn on the silicon surface (C), on the apparent surface viewed through the glass (B), and on a thin mark on the upper glass surface (A). The refractive index was calculated from $n = \frac{\text{actual thickness}}{\text{apparent thickness}} = \frac{AC}{AB}$. The same principle could be used for bulk glass, or for thin layers, with suitable changes in the precision of the calibrated scale used. For thin layers, the objective focusing drum was graduated in microns. With this method the refractive index of zinc alumino borosilicate glass was found to be 1.6, and that of the borosilicates approximately 1.5. (See also Section 5.2 below for another measurement of n.) Once n was known, this same method could be used to determine layer thickness ($AC = n \cdot AB$). With practice, reproducible focusing could be obtained on the lapped surfaces with an average roughness of 5 microns generally used in this work. If thin evaporated contacts were present on the lapped surface, they could also be used to give the focus position. On polished slices, polishing scratches were convenient for focusing. The top of the glass layer (A) was located by focusing on a thin mark made with a wax pencil on the surface.

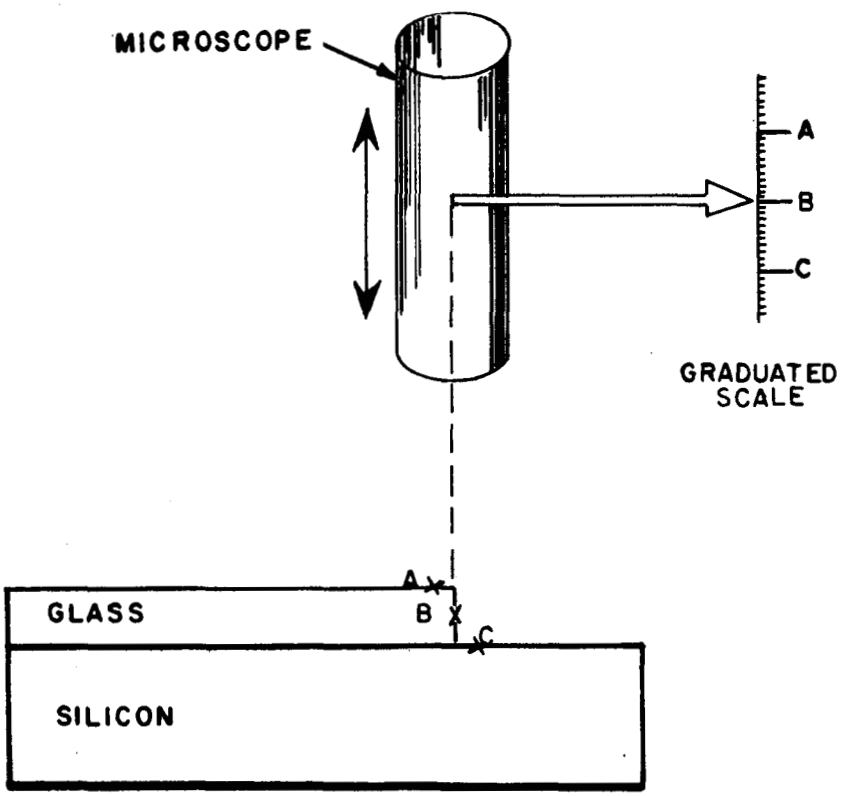


FIGURE I

THICKNESS MEASUREMENT BY DIFFERENTIAL FOCUSSING METHOD (DIAGRAMMATIC)

This method allowed rapid measurement of the thickness, and of variations across the cell surface. The accuracy of focusing for layers 25 microns thick was ± 3% for positions A and B. Generally at least three measurements were taken for each sample, and averaged. The measured variation of these average thicknesses was ± 1.5 microns, except near to the edges, where the layer thickness fell to half the average value. Most of the variation was caused by the drying patterns of the slurry.

Control

Typical curves of the variation of slurry transmission versus wavelength are given in Figure 2. Figure 3 shows the change in transmission at fixed wavelength 750 millimicrons, versus time. This change is seen to be insensitive to the starting transmission, and thus no additional information on the glass particle size population could be gained from these curves. The stability of the colorimeter is seen in Figure 3 by the plot of a standard solution of isopropyl alcohol and ethyl acetate.

Figures 4 and 5 show the basis of the empirical thickness control using the above thickness measurements, and slurry transmission at 750 millimicrons. Figure 4 shows the measured thickness of the resultant fused layers versus the 750 millimicrons transmission of the slurry used. Figure 5 (a) shows the actual glass density, obtained by weighing the glass in a dried known volume of slurry as a function of the transmission. Figure 5(b) shows that there is a good approach to the expected linear relation between the layer thickness and the slurry density. Examples of the successful degree of control achieved are given below, in particular in Section 5.7.

5.2 Topography And Imperfections

In preliminary studies, it was found that for very thin layers, defects in early films were filled in on subsequent layers. Figure 6 shows 1, 2 and 3 coats of a low density slurry on a polished slice. In Figure 6(a) about half the slice area is covered with glass. In Figure 6(b), the glass layer is continuous except for a few holes (approximately 1 micron diameter). In Figure 6(c), the hole density has fallen by a factor of five. For thicker slurries the holes were completely removed with successive layers. Figure 7 shows the fill-in for

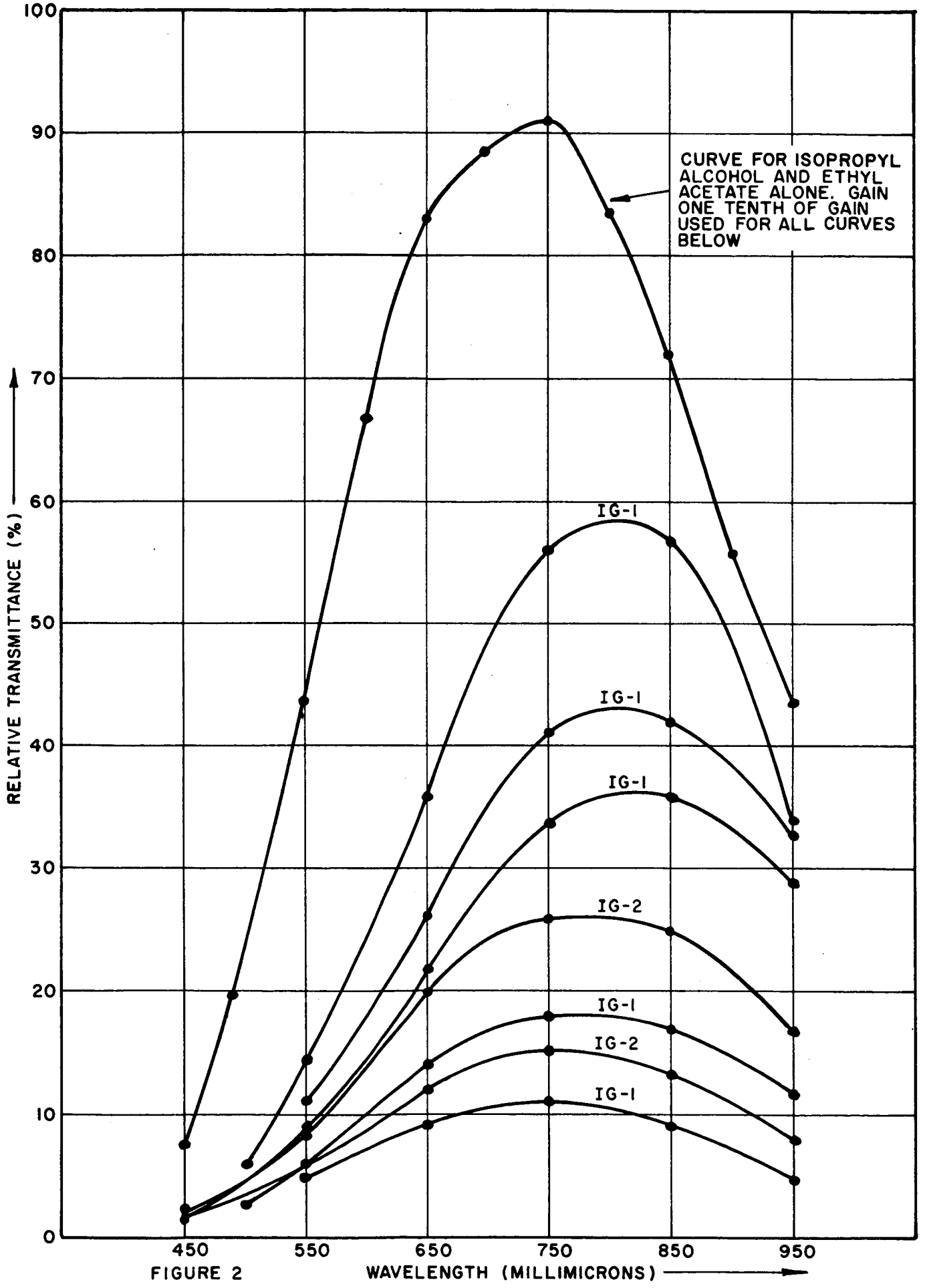


FIGURE 2

RELATIVE TRANSMITTANCE OF SLURRIES AS A FUNCTION OF WAVELENGTH

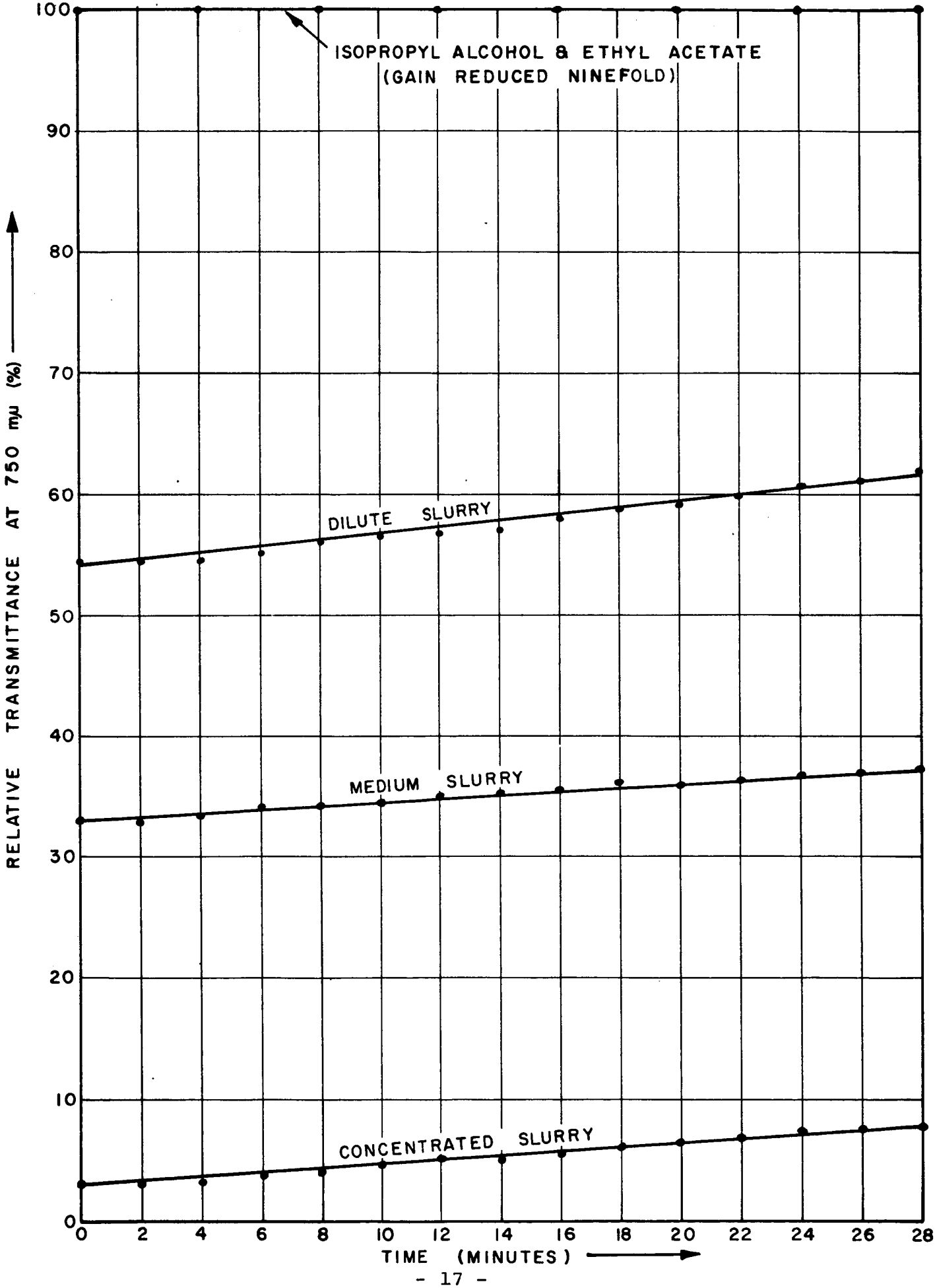


FIGURE 3 - RELATIVE TRANSMITTANCE MEASUREMENTS AS A FUNCTION OF TIME

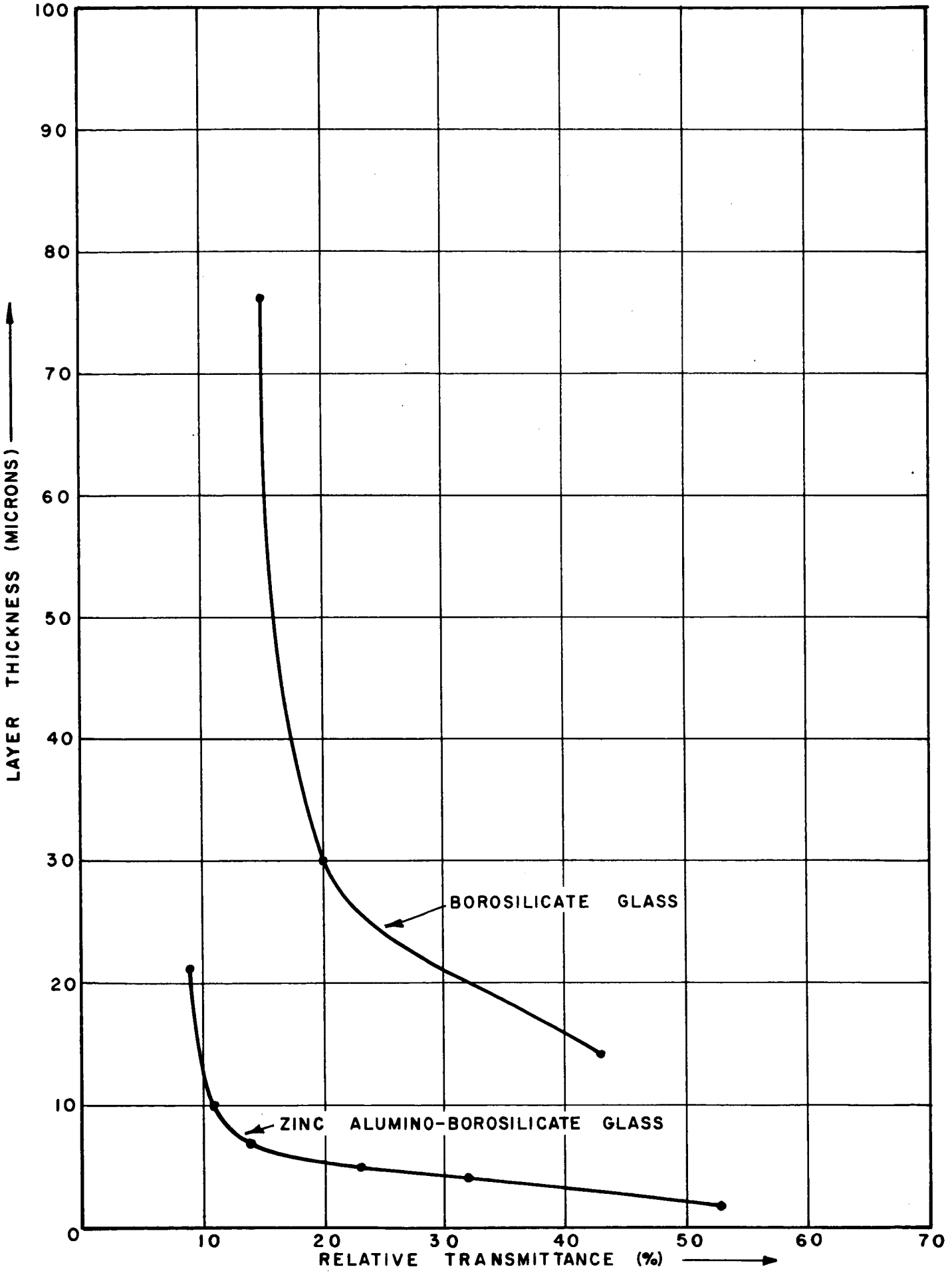


FIGURE 4 LAYER THICKNESS AS A FUNCTION OF SLURRY TRANSMITTANCE

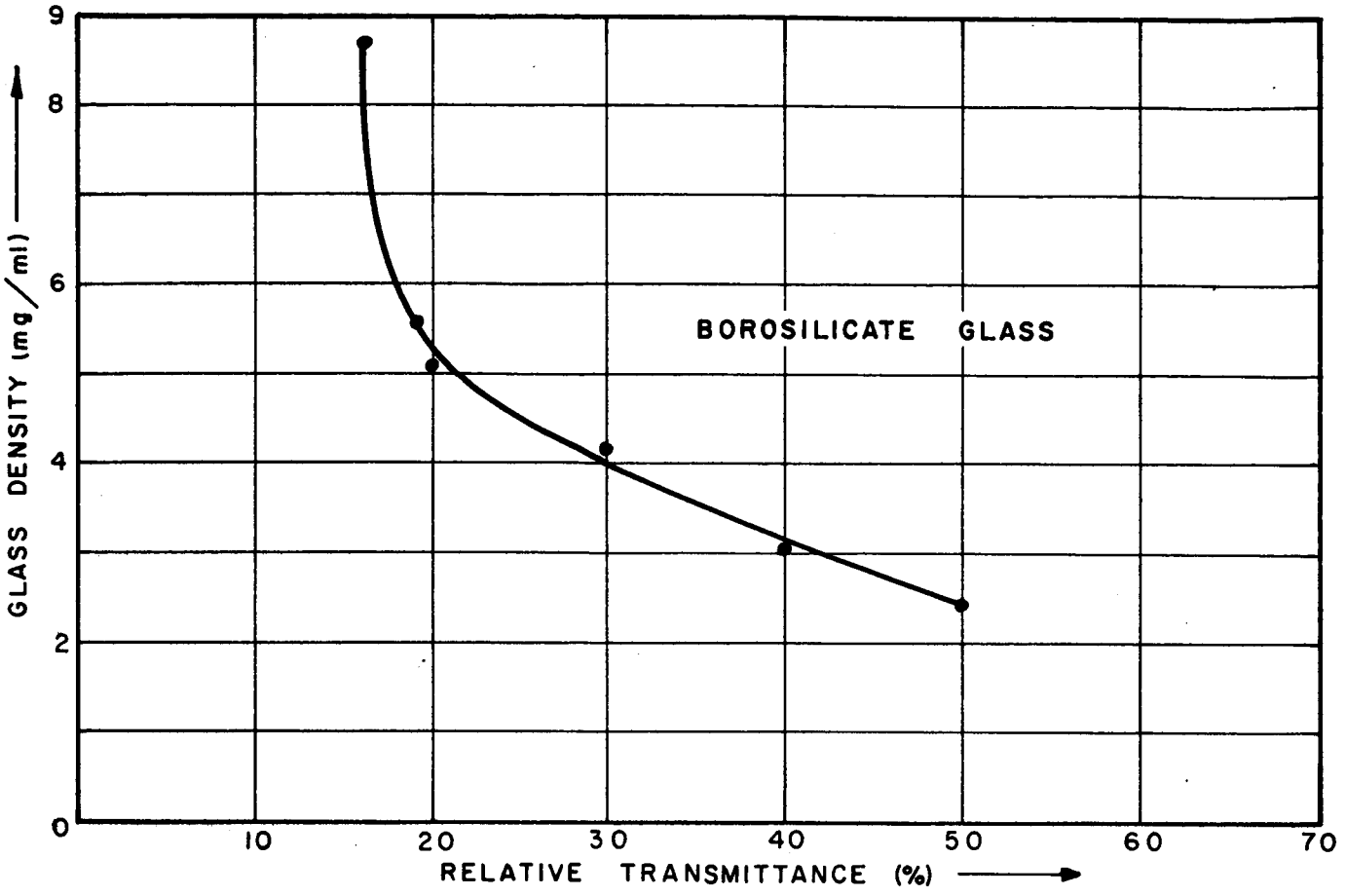


FIGURE 5a ACTUAL DENSITY VERSUS RELATIVE TRANMITTANCE

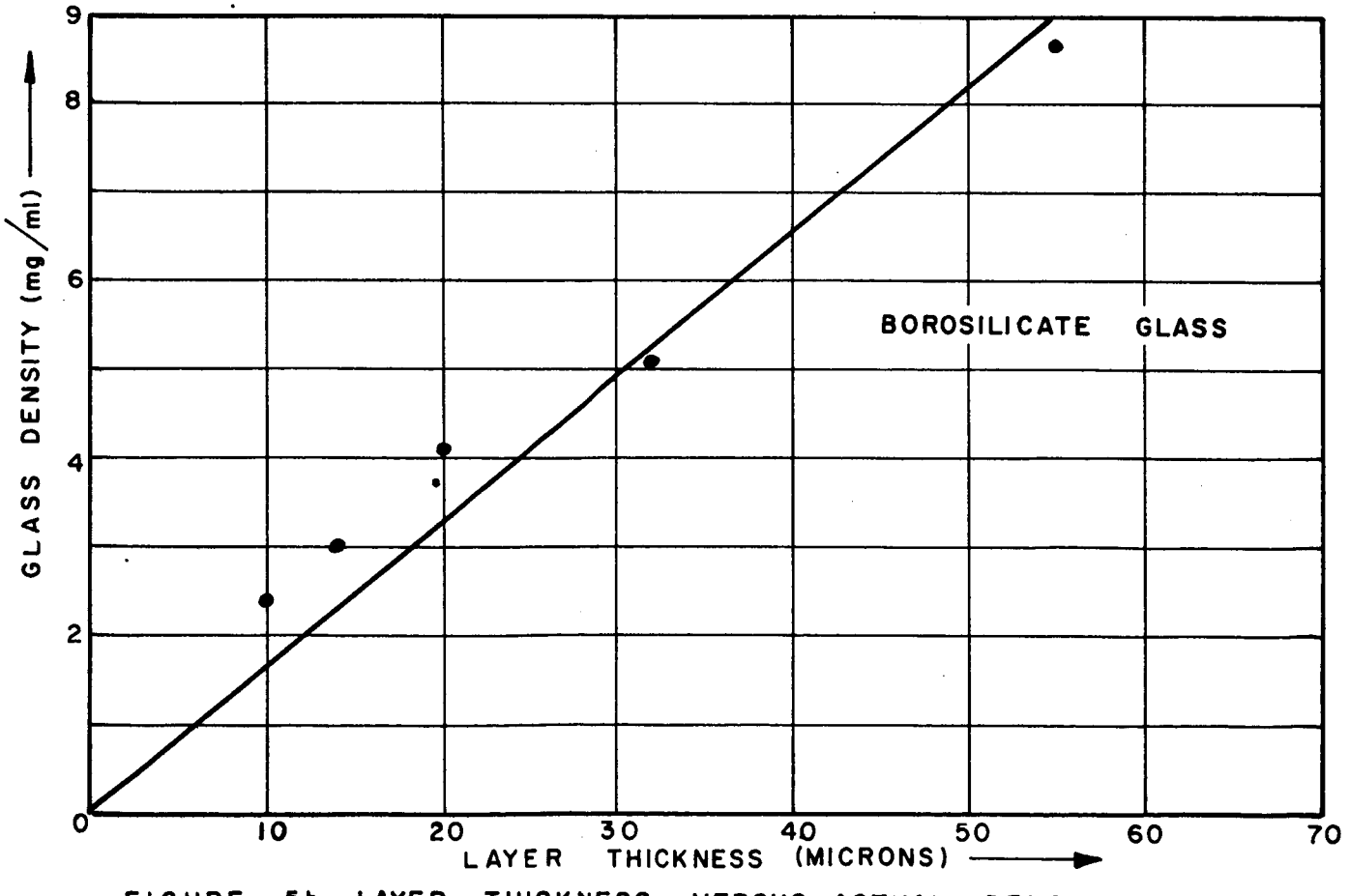
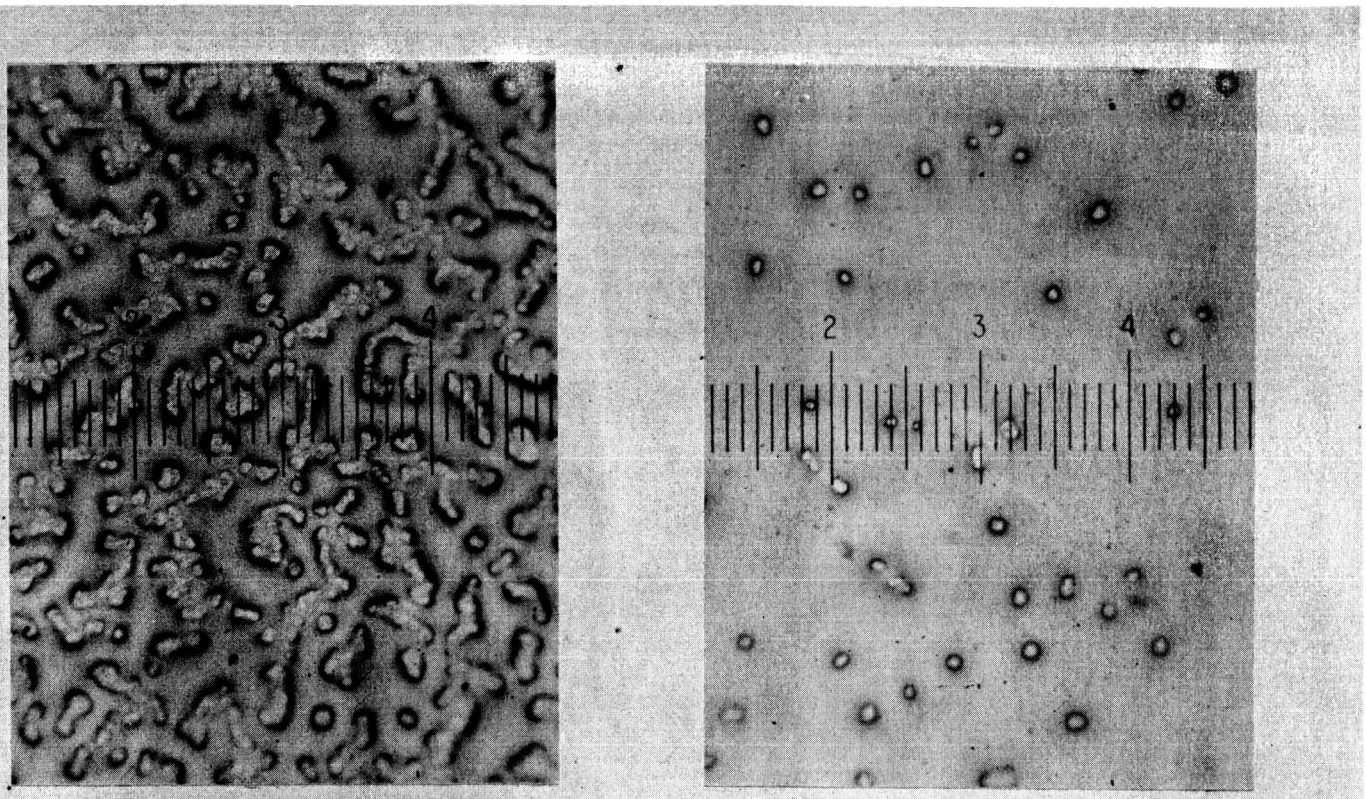
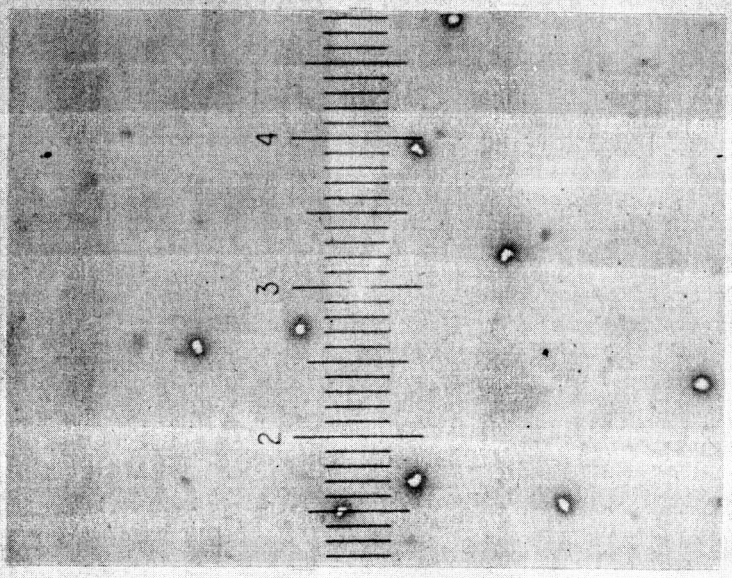


FIGURE 5b LAYER THICKNESS VERSUS ACTUAL DENSITY



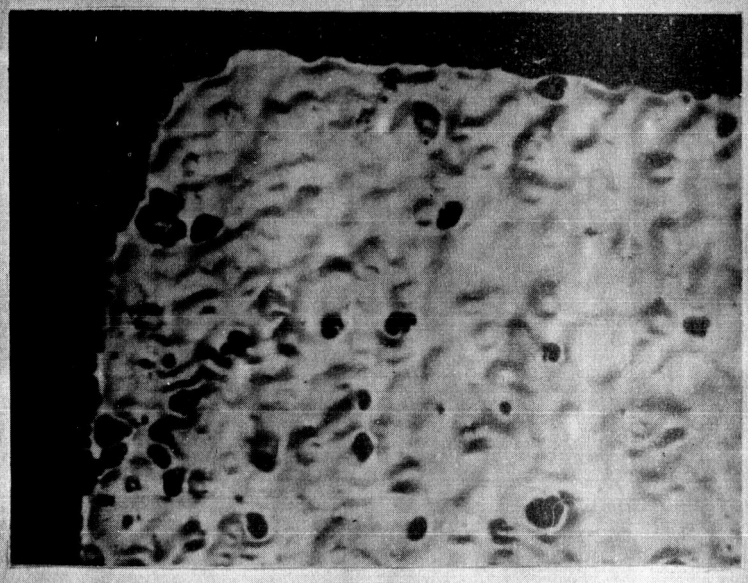
(a)

(b)

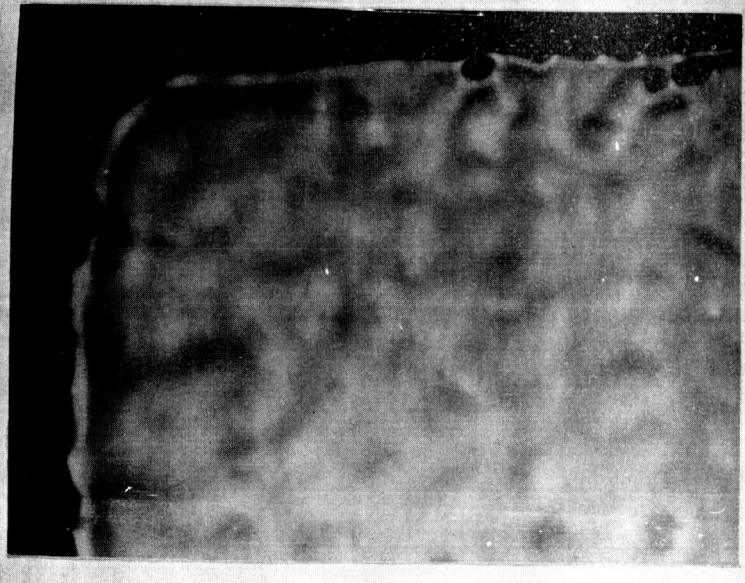


(c)

FIGURE 6 - PHOTOGRAPHS (300X) SHOWING GLASS LAYER FILL-IN FOR THIN LAYERS



(a)



(b)

FIGURE 7 - PHOTOGRAPHS SHOWING GLASS LAYER FILL-IN FOR THICK LAYERS.

a lapped slice for 1 and 2 coats of denser slurry. An interesting observation was that as fusing was more complete, the cooled glass surface became flat. In fact for good glass layers, around 1 mil thick, even on a rough lapped surface with average roughness between 1/5 and 1/10 mils, interferometric investigation showed the glass layer to be much flatter than the starting silicon surface. Examples of this are shown in Figure 8. Figures 8(a) to 8(d) show interference photographs for 4 lapped slices, using a single slurry, giving a thickness around 1 mil, when the fusing time was varied. In all four cases, the voltage was kept constant for the heating strip, to give a maximum temperature around 830°C, and the total heating times were 15, 20, 30 and 60 seconds. The general improvement in topography can be seen by the wider spacing of the fringes. There are signs of local irregularities a few microns different from the surrounding surface (shown by the terraced fringe patterns). These are generally raised portions from inclusions like dust, unfused glass, or from unmelted particles of alumina introduced during the milling process. Some defects are shallow pits left on cooling.

Figure 9(a) shows an example of a good glass layer formed under the same conditions, but with the heating stopped immediately fusion appeared to be complete. Figure 9(b) shows a mechanically polished slice partly covered with a glass layer. Apart from the pronounced curvature at the boundary, the parallel fringe lines on the polished surface are seen to be generally continued on the glass side, with deviations caused by small local irregularities.

Figure 10(a) shows a cleaved section of a lapped slice with a glass layer around 35 microns thick. The lower reflectivity of the glass layer is apparent, the cleaved silicon which is seven times as reflecting, being the bright portion with cleavage lines. The shiny skin on the glass layer can be seen (indicated by the arrow). Figure 10(b) shows the same section after the slice was dipped in hydrofluoric acid for 10 seconds. The matte surface described above was left, and the layer was about 5 microns thinner. The shiny skin can be seen to be removed. The lighter appearance was caused by the photography, the actual samples having about the same reflectivity. If this matte glass surface was fused again, the shiny surface re-formed, showing it to be a surface effect. Figure 11 shows other imperfections

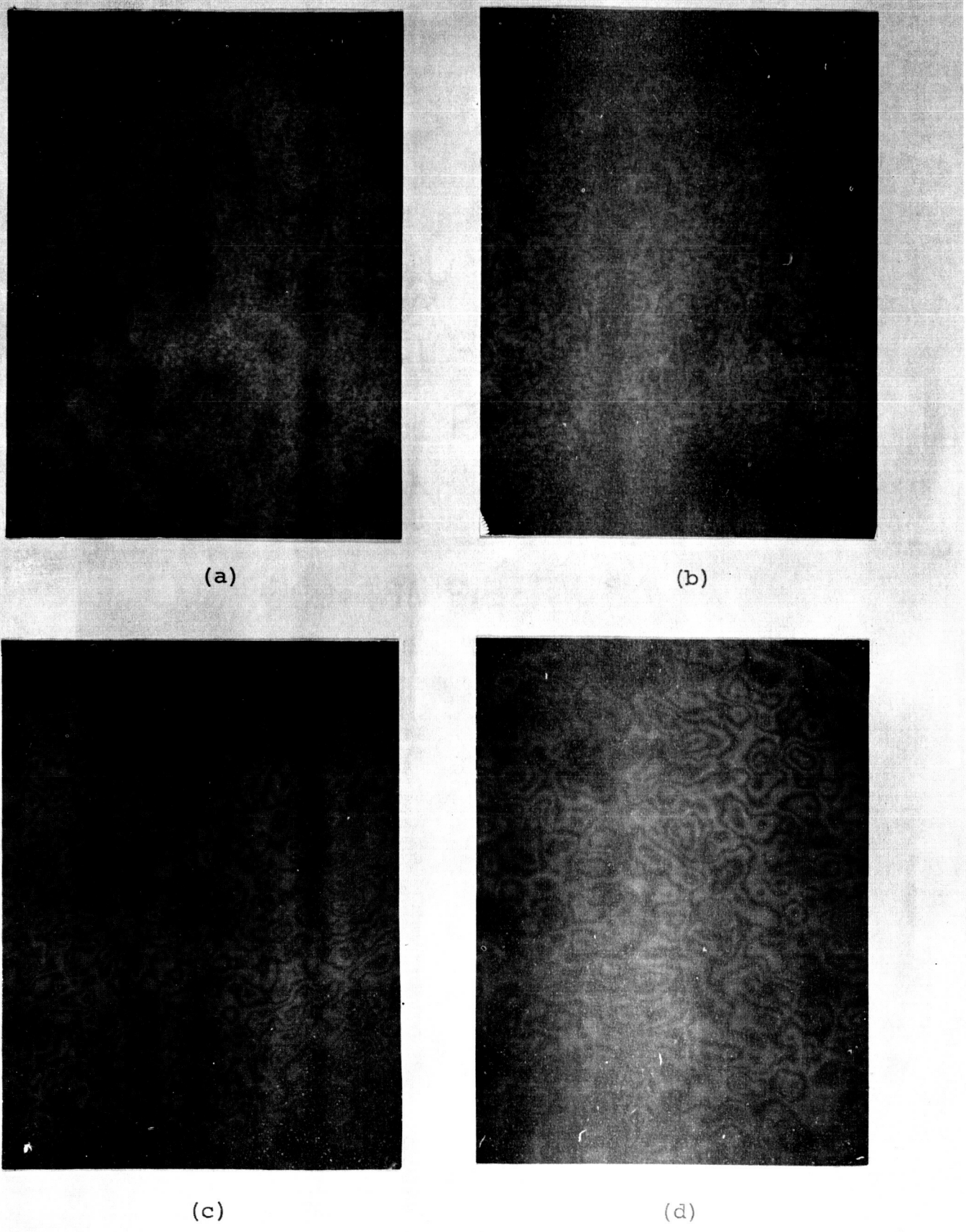
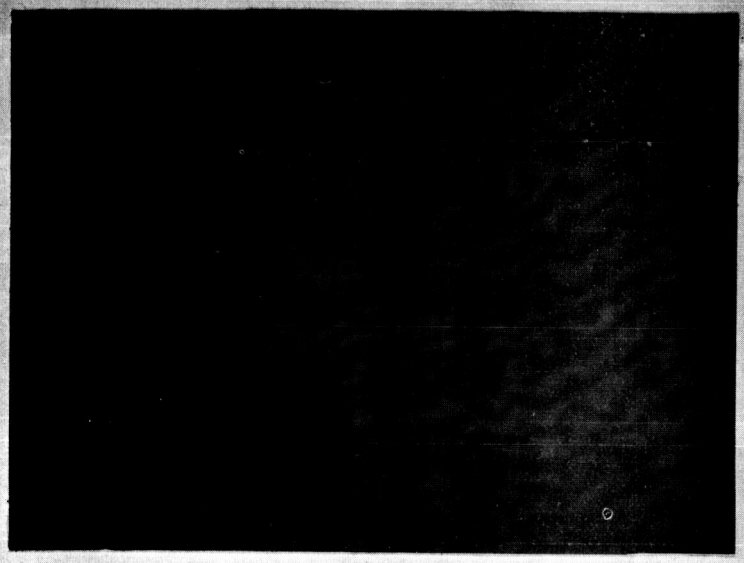
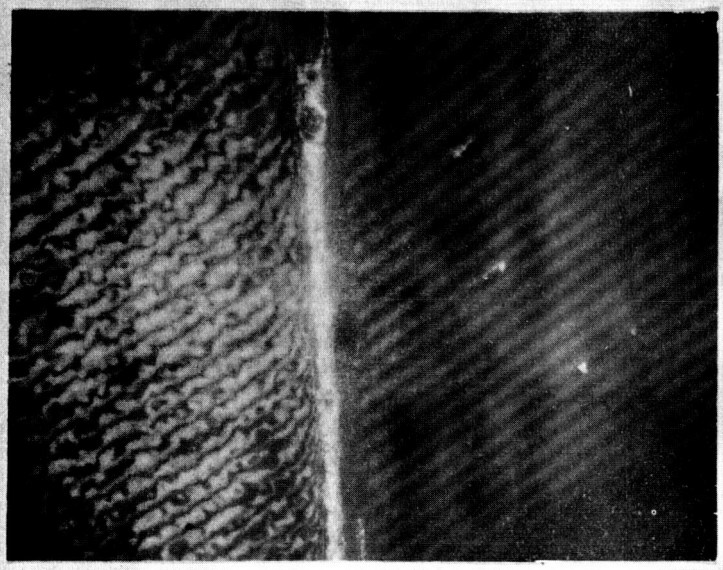


FIGURE 8 - INTERFERENCE PHOTOGRAPHS (75X, SODIUM LIGHT) OF GLASS SURFACES AS HEATING TIME WAS INCREASED



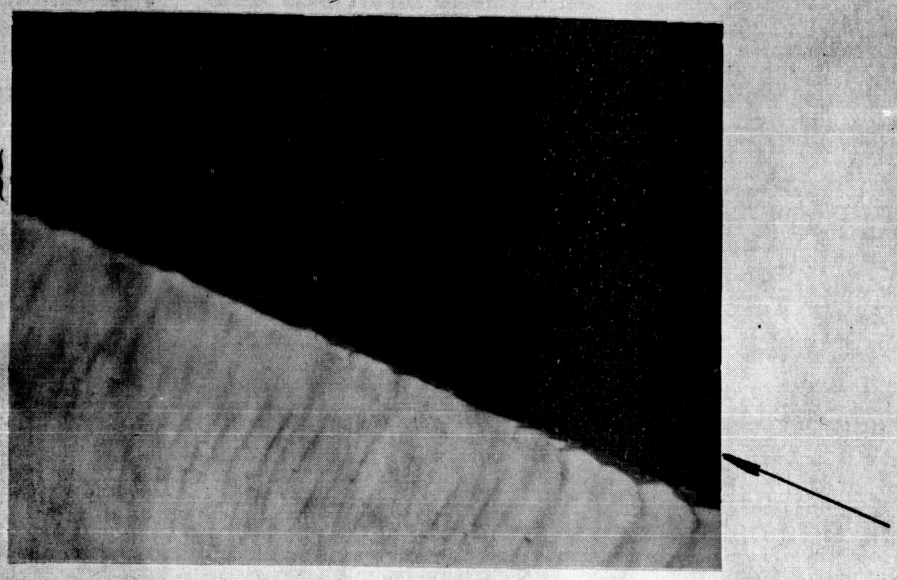
(b) LAPPED SILICON



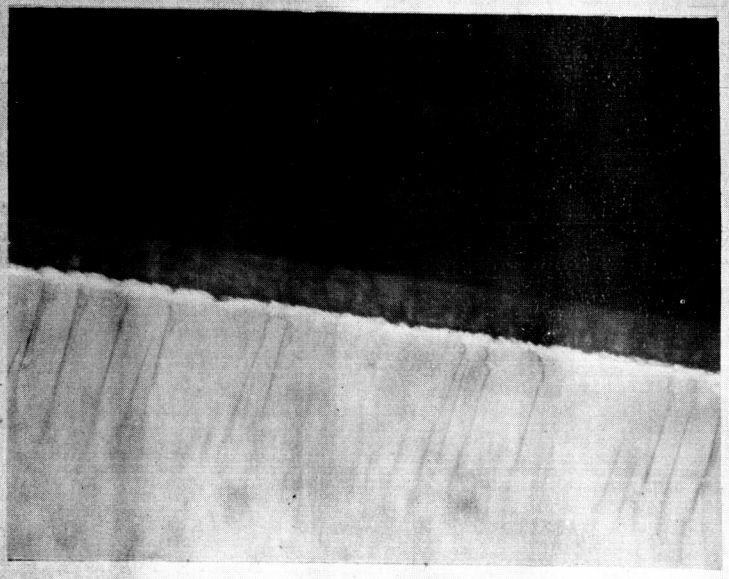
GLASS NO GLASS

(a) POLISHED SILICON

FIGURE 9 - INTERFERENCE PHOTOGRAPHS (75X, SODIUM LIGHT) OF GOOD GLASS SURFACES

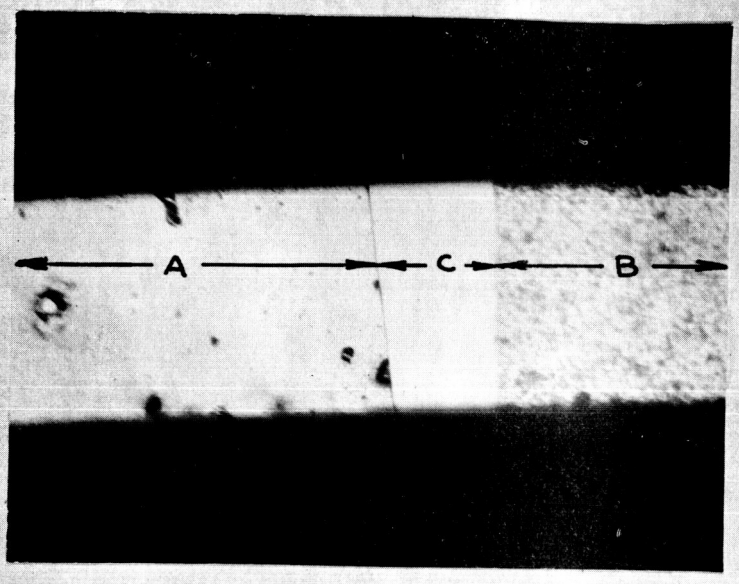


(a) SHINY SURFACE

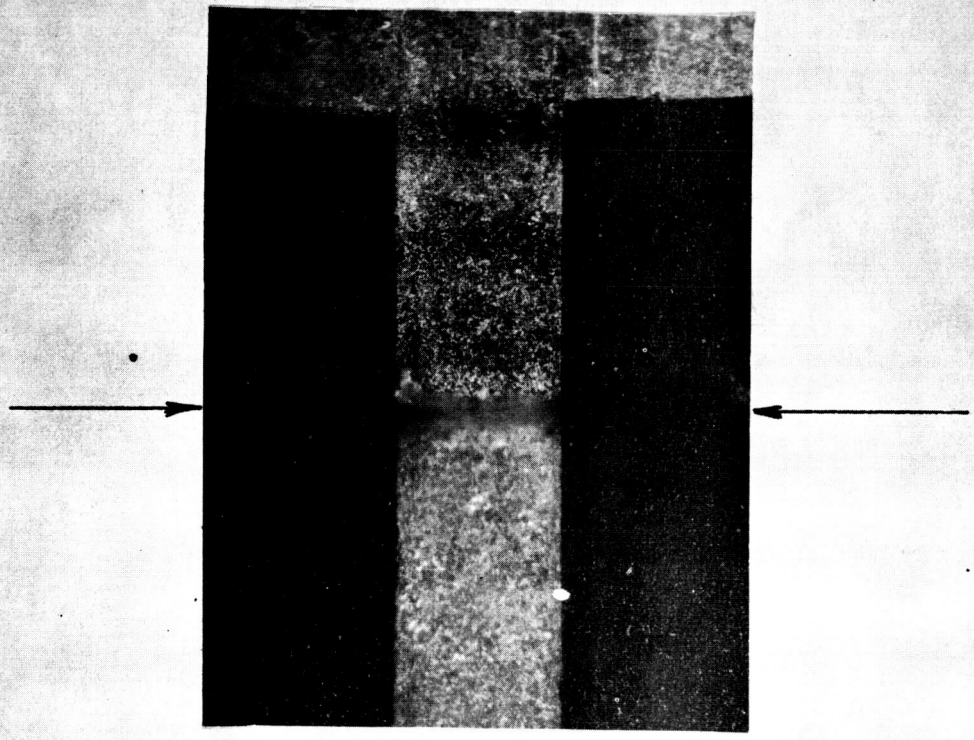


(b) MATTE SURFACE

FIGURE 10 - PHOTOGRAPHS (300X) OF CLEAVED SECTION OF SILICON SLICE WITH GLASS LAYER



(a) TRANSMISSION PHOTOGRAPH



(b) FUSED GLASS ON CELL

FIGURE 11 - PHOTOGRAPHS SHOWING TRANSPARENCY OF FUSED GLASS

but the same photographs show that the glass layer was generally of high quality. Localized imperfections appeared as tiny bubbles, caused during fusion. These bubbles generally did not extend through the whole layer, and for multiple layers, they were confined within each layer. The number of bubbles could be reduced by using finer glass particles in the slurry, and by not exceeding the temperature at which localized bubbling increased drastically.

Discussion on the measured transparency of the layers is given below in Sections 5.5 and 5.6. The photograph shown in Figure 11a shows some of the imperfections but also illustrates the degree of transparency of the fused layers. The samples for this photograph were formed either on silicon or Kovar, and then removed. For the former case, the slice was mounted glass side down in wax, and the silicon was removed by etching in approximately equal parts of nitric and hydrofluoric acids. With care, the etching could be stopped before the hydrofluoric acid attacked the glass. The latter layers were deposited on 2.5 mil thick Kovar strip, and then removed by flexing the Kovar. This method did not produce such large sheets as the etching away of the silicon, but was interesting in showing the good flexibility of the glass layer before it broke away. Figure 11a shows a transmission photograph through a sheet (A) of borosilicate glass fused around 950°C, and through another sheet (B) of the same glass fused at the usual temperature (880°C). Between these sheets is an air gap (C). Sheet A is seen to be highly transparent but with a few large imperfections. With these thin sheets, the refractive index of the fused glass could be measured by another method. In this, the glass sheets were immersed in a series of liquids of graduated refractive index, until the lack of visibility of the glass showed that the refractive index of the liquid matched that of the glass. In this way, the index values given above were confirmed.

Figure 11b also shows the transparency of the layers. It is a magnified picture (120 X) of the intersection of a grid line and edge contact of a cell. The fused glass did not reach the edge contact, and the boundary is shown by the arrows. Comparison of the appearance of the evaporated grid line on either side of this boundary shows the transparency.

5.3 Thermal Emittance Results

One of the major objectives of this work was to establish the effectiveness of the integral coatings for thermal control in space. The factor determining this effectiveness is the thermal emittance (ϵ), and to measure this quantity, conventional methods were adapted. Details of the method used, and some typical measurement results are given in Appendix I. The four cells best matched in glass thickness from groups of eight, were mounted on the brass sample blocks.

Table 2 gives details of the samples used, and Figures 12 and 13 summarize the experimental values of the emittance versus equilibrium temperature. Figure 14 shows the variation of the emittance at 30°C, from Figures 12 and 13, plotted against the glass thickness covering the cells. From theoretical predictions (reference 8) it was expected that as the glass thickness increased, the emittance in Figure 14 would increase from the emittance of silicon, approaching asymptotically the emittance value of the bulk glass (0.95 for refractive index = 1.5). The general trend is seen to be in agreement with expectations. For both cell surface finishes used, the transition thickness where the glass layer had thermal properties resembling thick layers, was around 1 mil. More work is needed to explain the deviations measured for some of the thinner layers, which generally showed "bulk" behavior for layers thinner than 1 mil, because the glass layers used for these samples were very consistent in thickness. For example, thickness measurements on all four cells used for samples J, K and L showed the deviations to be less than $\pm$ 0.75 μ for all three cases. From the above measurements, two conclusions could be drawn: (a) the emittance of integral glass layers was comparable to that observed for bulk glass for layer thicknesses greater than 1 mil; (b) the emittance was partly dependent on the silicon surface finish and was also affected by the surface finish of the glass.

Conclusion (a) represented one of the hoped-for objectives in the present work, and showed that integral glass layers 1 mil thick or greater, should be adequate for thermal control in space. Conclusion (b) could be exploited for integral coatings, because the surface could readily be made matte.

TABLE 2. Details of Emittance Samples Used.

SAMPLE	CELL SURFACE FINISH	CELL COATING	EXPOSED CONTACT METAL	COVER	SAMPLE BLOCK ENDS	AREA OF UNKNOWN ϵ (cm^2)
a	Lapped	Ph-g[1]	solder	- - -	soldered	6.95
A	Lapped	Ph-g	solder	6 mils 0211	soldered	7.7
B	Lapped	Ph-g	solder	5 microns IG-1[2]	soldered	7.4
C	Lapped	Ph-g	solder	10 microns IG-1	soldered	7.4
D	Polished	SiO	silver	- - -	brass	7.3
E	Polished	SiO	silver	- - -	soldered	7.3
E'	Polished	None	silver	- - -	soldered	7.3
F	Polished	SiO	silver	6 mils 0211	brass	7.7
G	Polished	SiO	silver	30 microns IG-2[3]	brass	7.7
H	Lapped	Ph-g	silver	30 microns IG-2	brass	7.7
I	Lapped	Ph-g	silver	25 microns IG-2(matte)	brass	7.7
J	Lapped	Ph-g	silver	8 microns IG-2	brass	7.7
K	Lapped	Ph-g	silver	9.5 microns IG-2	brass	7.7
L	Lapped	Ph-g	silver	14 microns IG-2	brass	7.7
L'	Lapped	Ph-g	silver	14 microns IG-2	brass	7.7
L"	Lapped	Ph-g	silver	9 microns IG-2(matte)	brass	7.7

(1) Ph-g refers to an antireflection coating of phosphosilicate glass, produced during diffusion.
(2) IG-1 is zinc alumino borosilicate glass.
(3) IG-2 is borosilicate glass.

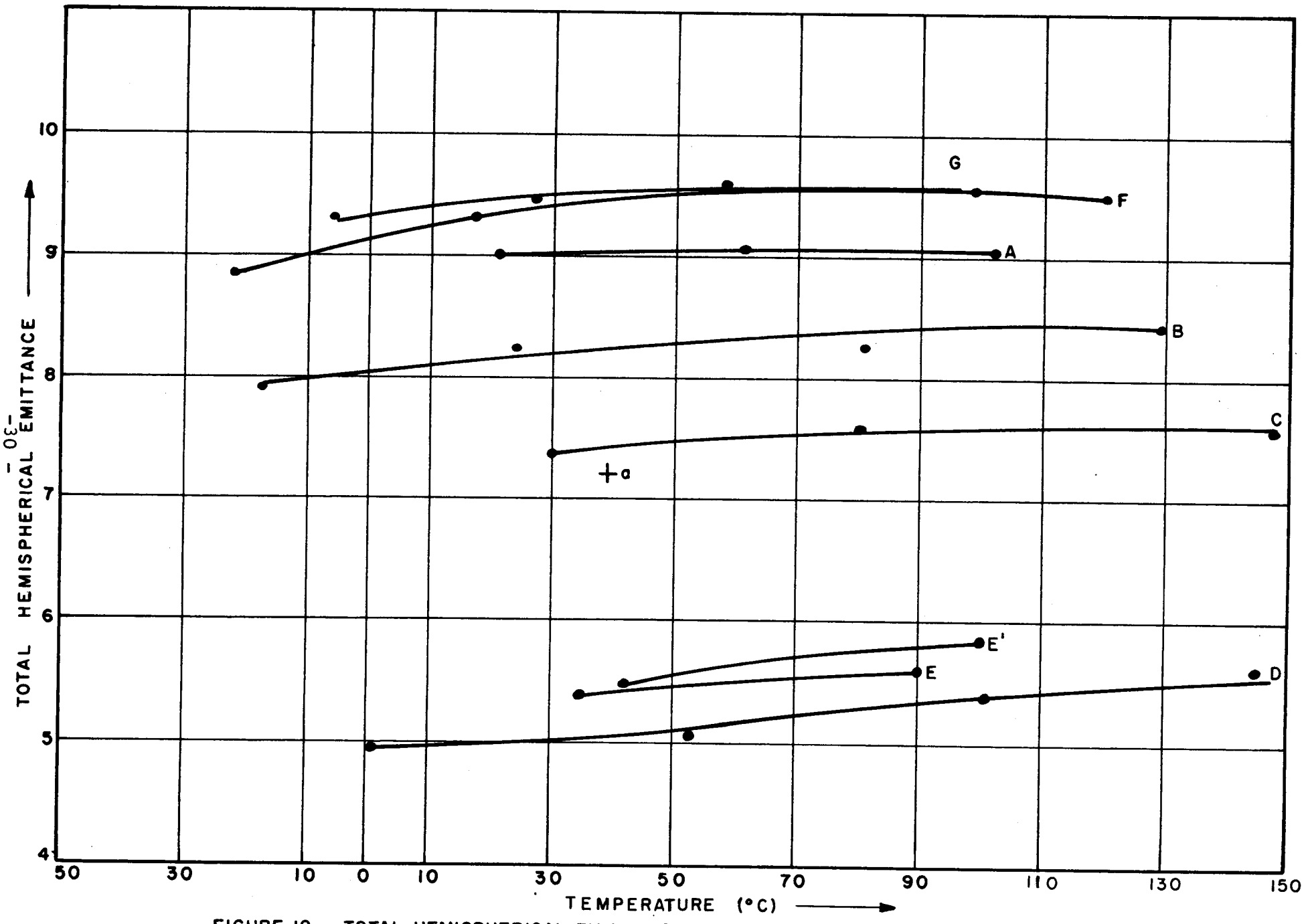


FIGURE 12 — TOTAL HEMISPHERICAL EMITTANCE AS A FUNCTION OF TEMPERATURE

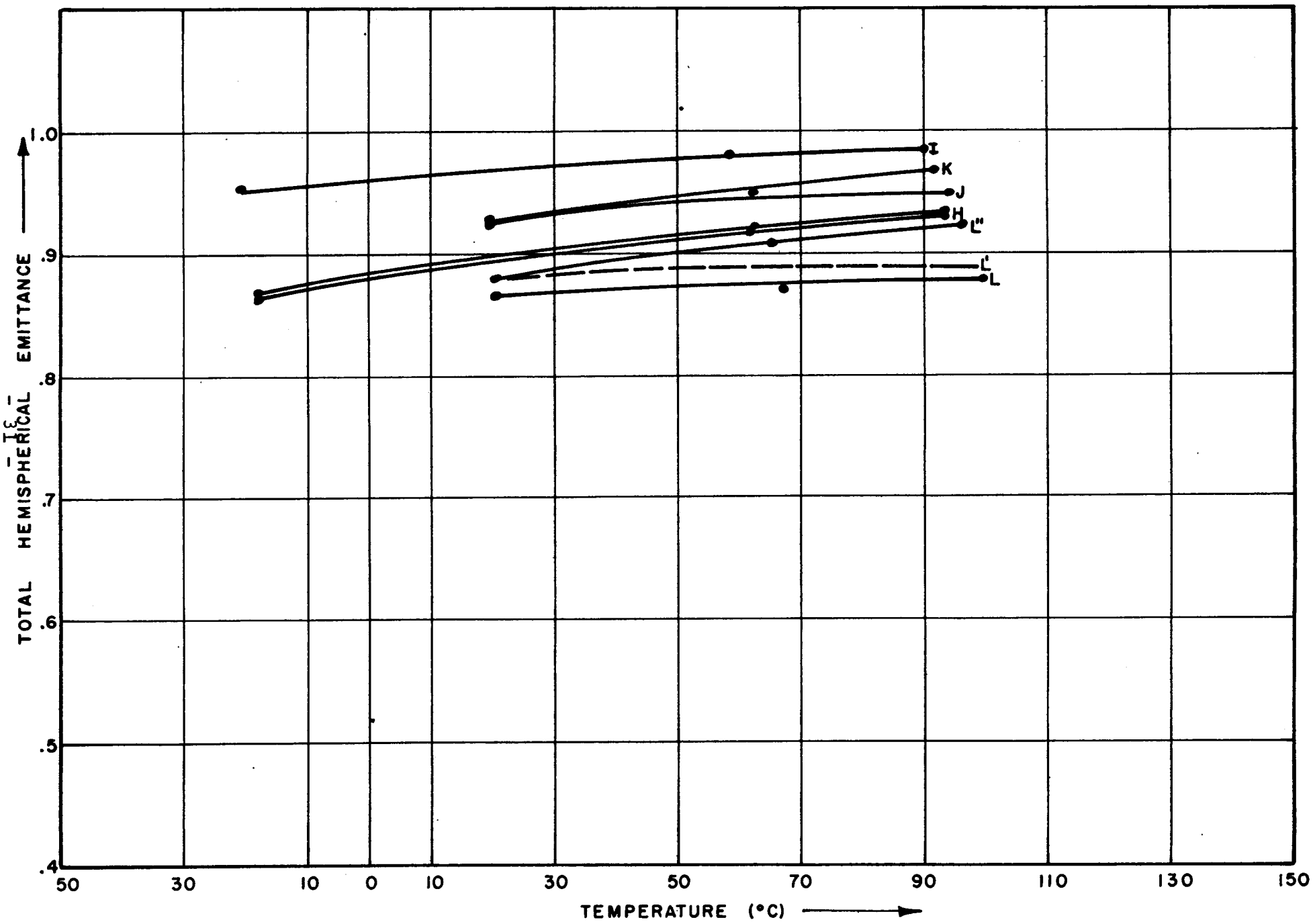


FIGURE 13 TOTAL HEMISPHERICAL EMITTANCE AS A FUNCTION OF TEMPERATURE

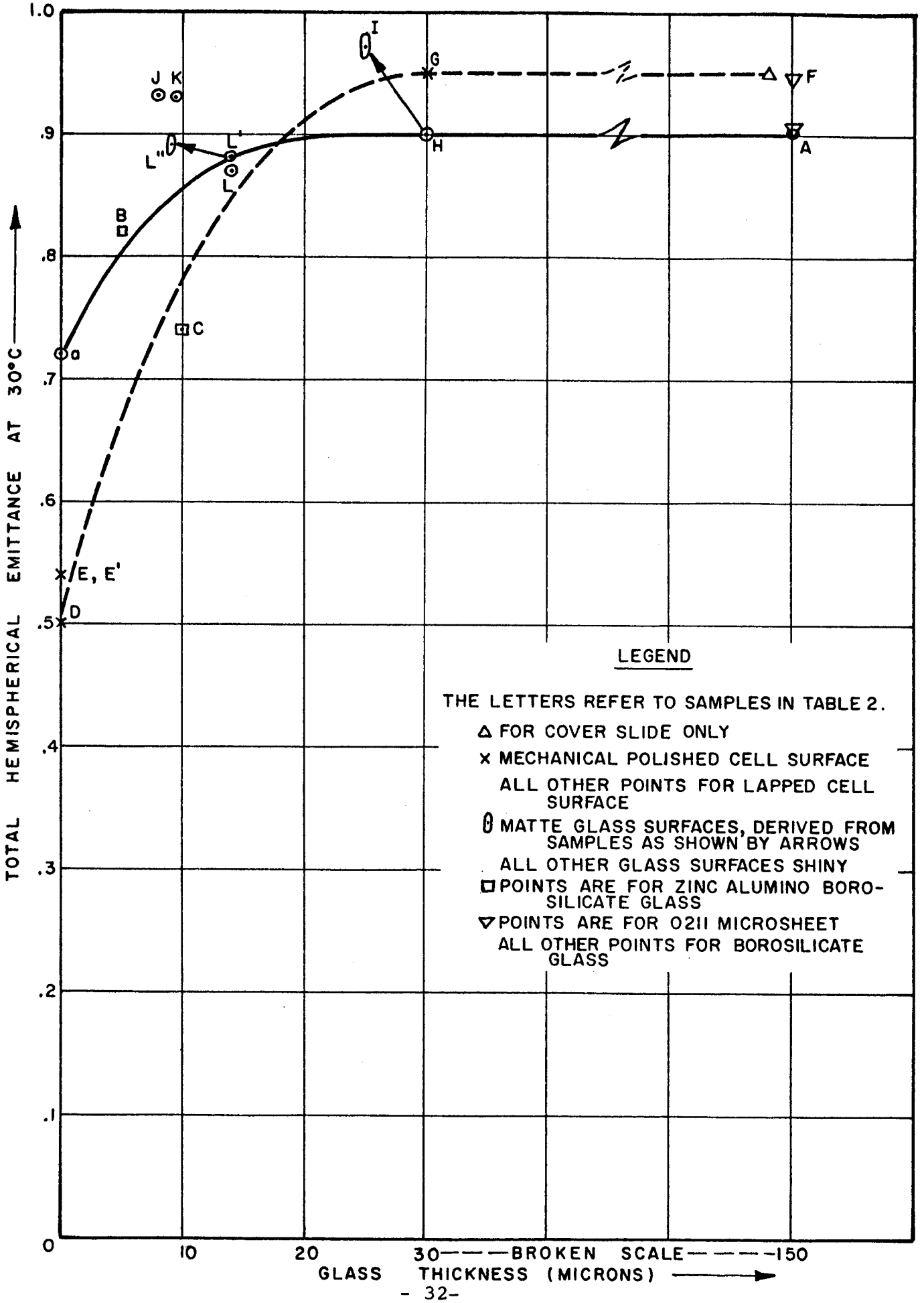


FIGURE 14 – EMITTANCE AT 30°C AS A FUNCTION OF GLASS THICKNESS

5.4 Solar Cell Characteristics

Measurement of the output of coated solar cells yielded much information on the interaction between the layers and the cells. Both the glass layers and the fusion cycle could have adverse effects on cell output. Before discussing the methods used to minimize these effects, a brief survey of possible effects is given.

The characteristics most often measured on coated cells were the photovoltaic I-V curve, the dark reverse current of the cell, and the spectral response. The most realistic light source used for the I-V output was one reproducing space sunlight, and here, the performance under the Hoffman Solar Simulator was the final criterion. However, for evaluating fabrication processes, a controlled tungsten source was more convenient.

Figure 15 shows a photovoltaic curve, reflected from the fourth to the first quadrant for convenience, for a solar cell at a fixed temperature, illuminated by a source of fixed spectrum and intensity. Four points of interest on this curve are shown. I_{SC} is the short circuit current, the maximum current generated in the cell. V_{OC} is the open circuit voltage, the voltage developed across the open cell terminals. At P_{max}, the maximum power point, the product of current and voltage is a maximum. A is a typical test point, showing the current I_1 at a fixed load voltage V_1. The values of these four points depended on the detailed cell properties, but some general rules are given to show how cell performance, or degradation, could be evaluated from such curves.

Short Circuit Current

The value of I_{SC} for a constant light source, depended on the reflectivity and active area of the cell surface, and on the effectiveness of collection of the generated carriers, both in the shallow N+ top layer, and from the bulk P-silicon. The N+ layer depth was maintained constant by close control of the diffusion process forming the PN junction. The bulk collection depended on the mean lifetime of the generated electrons, and the lifetime in turn depended on the resistivity of the

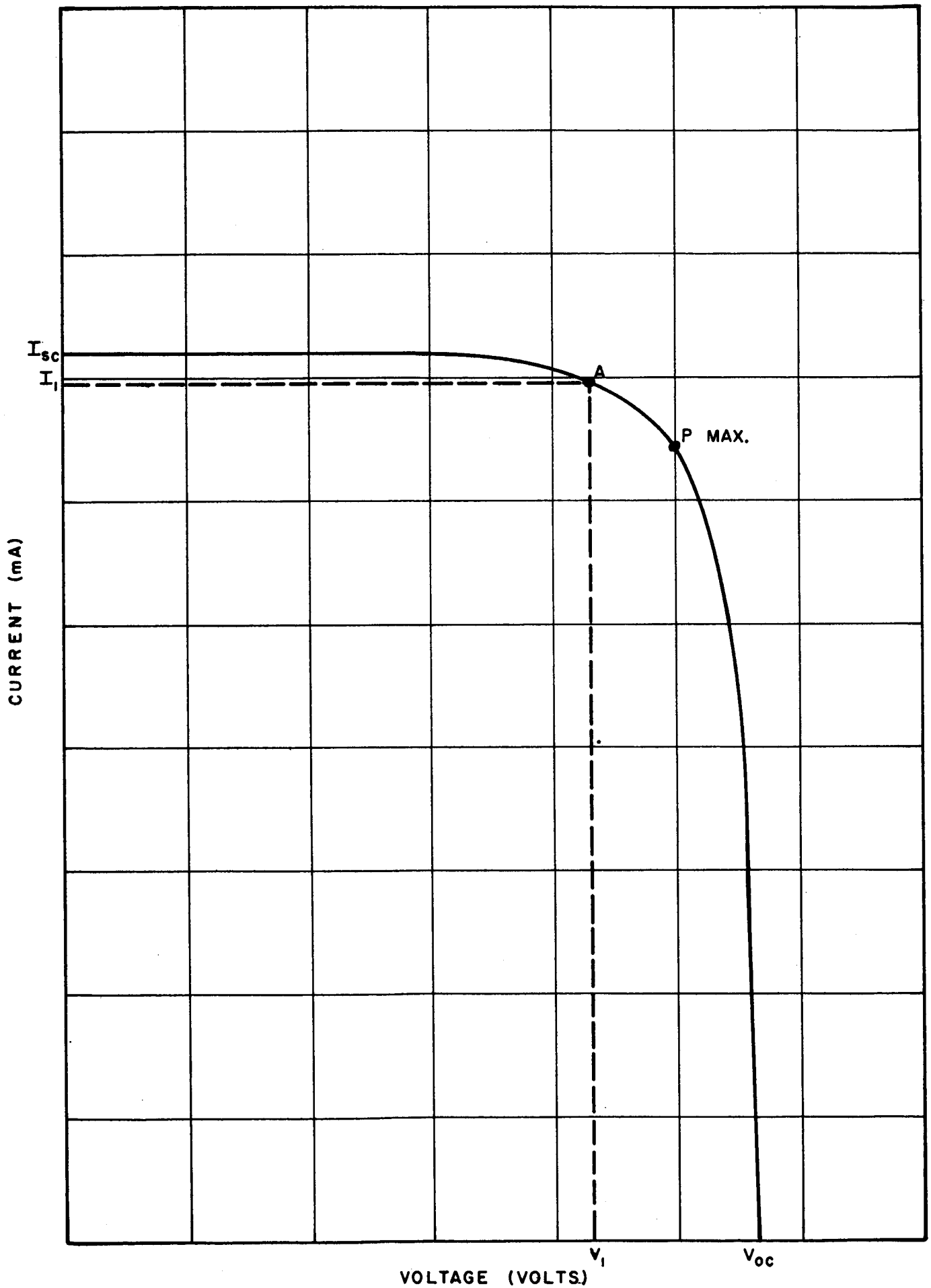


FIGURE 15 – SOLAR CELL PHOTOVOLTAIC I-V CURVE

silicon, and on the number of harmful trace impurities or thermal stresses introduced into the silicon during crystal growth or during diffusion. In addition, the fusing of a glass layer could reduce lifetime by impurities introduced from the glass, or by stresses during cooling, caused by mismatch between the glass and the silicon, particularly since the fusion temperatures were well above the range where silicon became plastic. Because there were fewer carriers generated at greater depths in the silicon, I_{SC} did not depend strongly on lifetime until this factor fell below 10 microseconds. I_{SC} also depended on the transparency of the glass coating, and when the other causes for variation of I_{SC} were known or removed, measurement of I_{SC} was a sensitive indication of the transparency of the fused glass layers. In this way, different slurry compositions, glasses or fusing cycles could be assessed quickly from the I_{SC} values, when I_{SC} for bare cells was known.

Open Circuit Voltage

V_{OC} depended on the resistivity of the bulk silicon, because this determined the Fermi level separation between the N+ and P regions. If the shunt leakage current across the cell was very high (and this would be shown by a high dark reverse current), V_{OC} could be decreased. V_{OC} also decreased for a poor PN junction characteristic under forward bias, and was temperature-dependent, decreasing approximately 2.3 mV/°C.

Series Resistance

The points P_{max} and A, for given values of I_{SC} and V_{OC}, were determined largely by the total series resistance of the cell. This resistance had three main components, the metal-silicon contact resistance at the back contact, the resistance at the top surface contacts, and the resistance of the bulk silicon. The second term was the resistance of the very thin sheet of N+ silicon modified by the presence of metal grids, which reduced the distance carriers must follow through the resistive sheet layer. One of the common configurations for a solar cell is shown in Figure 16; the three grid lines were thin (5 to 7 mils)

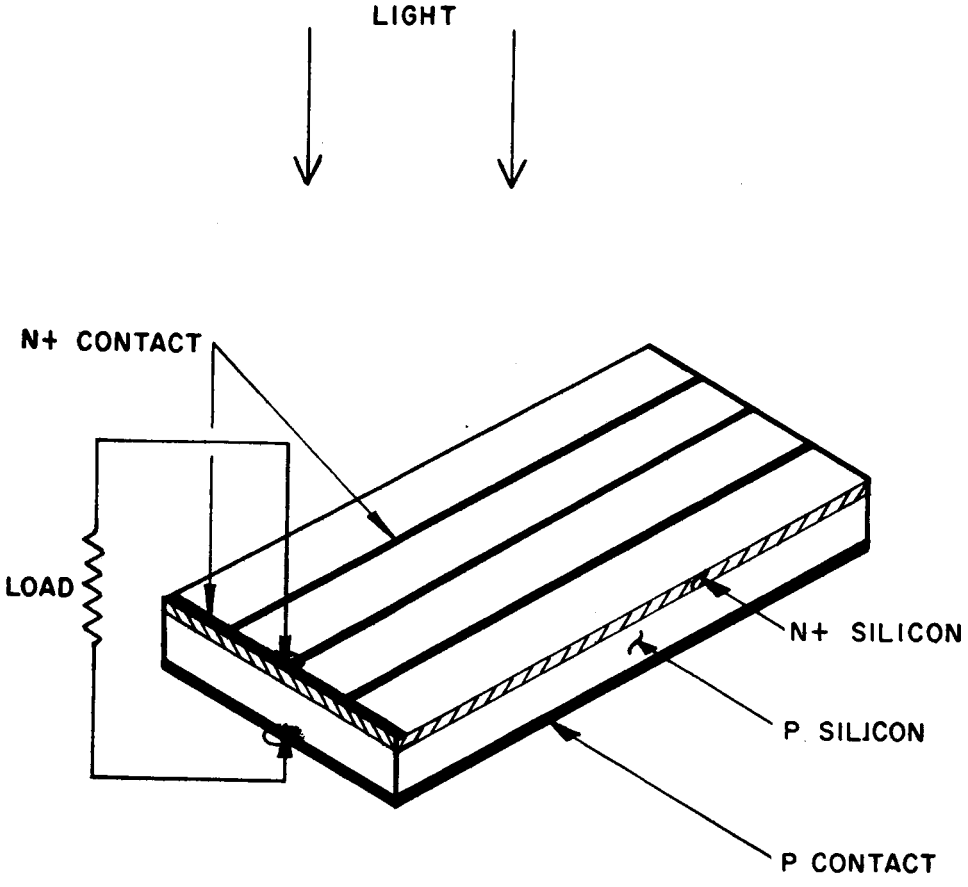


FIGURE 16

TYPICAL SOLAR CELL CONFIGURATION

and a good compromise between low sheet resistance and maximum active area, was achieved. The grid structure could also add two other contributions to the cell resistance. The resistance of the grid lines could be appreciable, and although the silicon directly under the top contact was highly doped, minimizing barrier formation, there could be non-Ohmic barriers formed by interaction between the contact metals and the cell surface layers. In Section 5.5(b) it is shown that the glass fusion cycle could lead to an increased contact resistance unless the contact structure was carefully designed.

Shunt Leakage

The points P_{max} and A were also affected by shunt leakage. There were three main causes of such leakage, namely, incomplete removal of metal particles or disturbed silicon around the edges of the PN junction, penetration of metal particles across the whole area of the shallow N+ region, and current generated at recombination centers in the space charge region of the PN junction. With good cleaning procedures, and care to minimize harmful impurities, the third cause could be kept small, and the first cause could be reduced by a good edge clean-up etch. The second cause, penetration by metal particles, took place only at elevated temperatures, high (> 600°C) for titanium and lower (400°C) for gold.

Spectral Response

The spectral response could show the effectiveness of collection of carriers as a function of wavelength. Early trials in this work compared the spectral response of a glass-coated cell and the same cell with the glass removed.

Figure 17 shows such curves. The relative cell response was similar for the two cases, showing that there was no selective absorption in the glass layer. Therefore any transparency losses were caused by a "flat" decrease in transmission over the wavelength range of interest (0.4 to 1.2 microns). Similar conclusions were drawn from the measured transmission losses of thick sheets of the glasses used, (see Section 5.6) although the cell spectral response comparison was more realistic, because it could reveal any unusual effects caused by the fused layers.

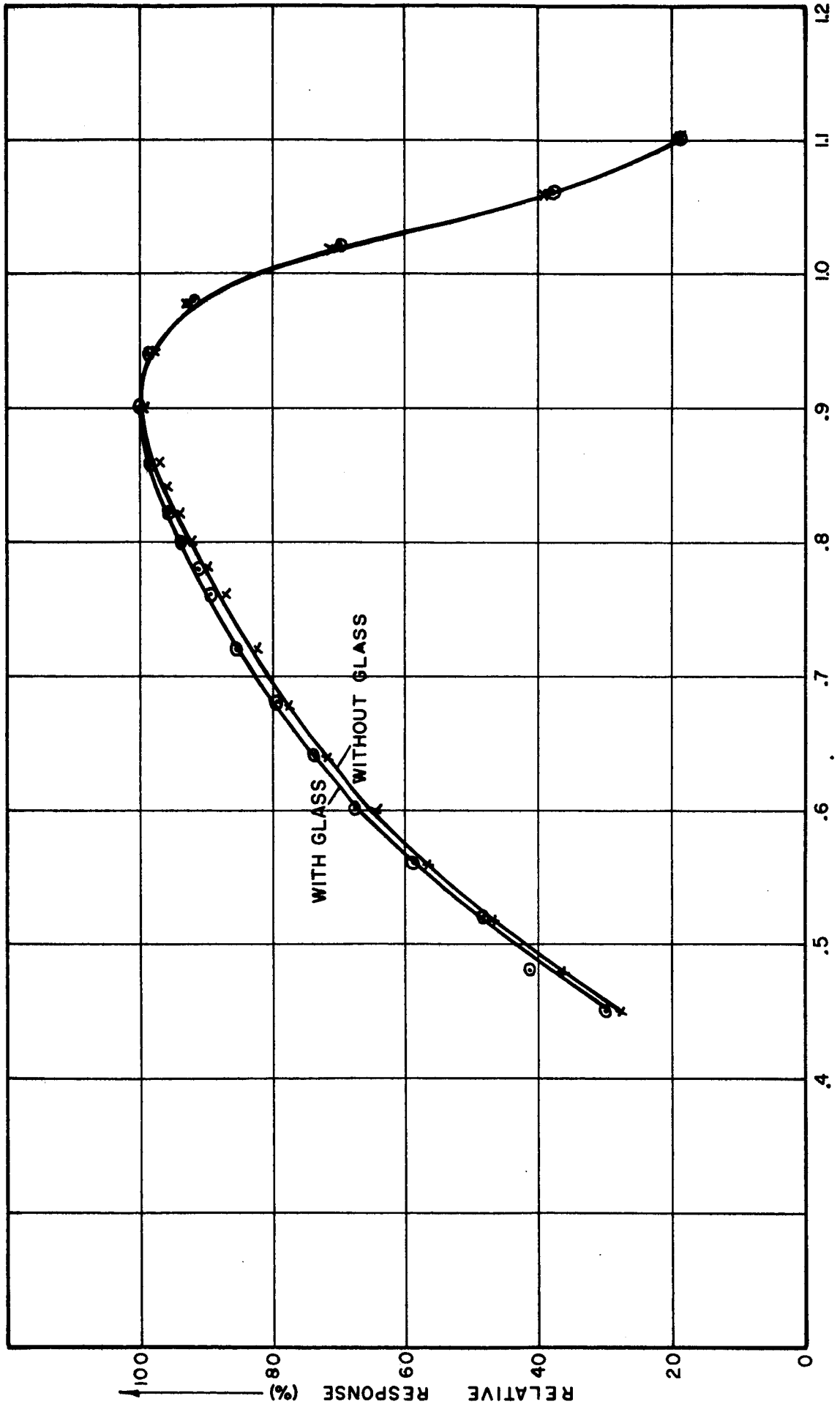


FIGURE 17 – RELATIVE SPECTRAL RESPONSE

5.5 Measured Results on Cells and Contacts

In this section a survey is made of the work leading to the present best state-of-art procedures (see Section 5.7).

For all the glasses used, much greater consistency, and higher I_{SC} and V_{OC} values were obtained when the glass was fused over the diffusion-produced phosphosilicate glass, rather than over the bare N+ - silicon. Another sign of interaction with the glass, showed as crazing of the layer between zinc-alumino borosilicate glass and silicon monoxide coated cells. The borosilicate glasses did not show this effect.

It was also shown that no appreciable change in I_{SC} resulted either from mechanically polishing the front surface of the glass layers, or from the matte surface formed in hydrofluoric acid.

a) Cell Measurements

At the outset, several factors which were not expected to vary during application of the glass layers, were checked on diffused slices. After fusing of the glass layers, no significant changes were found in the sheet resistance of the diffused N+ - silicon, in the resistivity of the P - silicon, or in the dark reverse current with or without titanium silver contacts on the back P - surface.

Minority Carrier Lifetime

Several diffused slices were divided into pieces, some pieces being kept as controls, others heated through the fusing cycle with no glass and others covered with fused glass. The glass was removed from the latter samples, and all three groups were plated on the sandblasted P-silicon, masked and etched to leave a number of N+ - plateaus on the diffused layer. The minority carrier lifetime in the P-silicon was measured for the plateau-diodes, by an electrical pulse recovery method. Typical results were as follows:

Diffused slice (control) - 14 microseconds
Diffused slice, heated only - 12 microseconds
Diffused slice, coated with glass - 11 microseconds

Considering the relatively severe heat cycle required to produce glass layers of high transparency, and with reference to the statement above that I_{sc} is not seriously decreased until the lifetime falls below 10 microseconds, these lifetime measurements suggested that good quality glass layers could be fused to cells without serious degradation of the cell properties.

Layer Build-Up Effects

With the zinc-alumino-borosilicate glasses, attempts to build up layers 2 mils thick, required up to seven successive layers. Although the output was fairly high, there was some degradation for the later layers, and the chance of degradation during repeated fusings was greatly increased.

With the borosilicate glasses, thicker single layers could be fused, and double layers as thick as 6 mils were formed. For one trial, the effects of layer build-up could be seen from the values measured under illumination by 2800°K tungsten, 100 mW/cm^2, with cells at 28°C.

	I_{sc} (mA)	P_{max} (mW)
Bare cell	59	20
Cell + 35 microns glass	54.3	19
Cell + 67 microns glass	52	18

In the samples used for irradiation trials (see Section 5.6), the thicker layers were built up by sequential layer fusions. The value of I_{sc} as a function of glass thickness is given in Figure 18. For zero glass thickness, the value for radiation batch R13 was used. The advantages of the borosilicate glass can be seen.

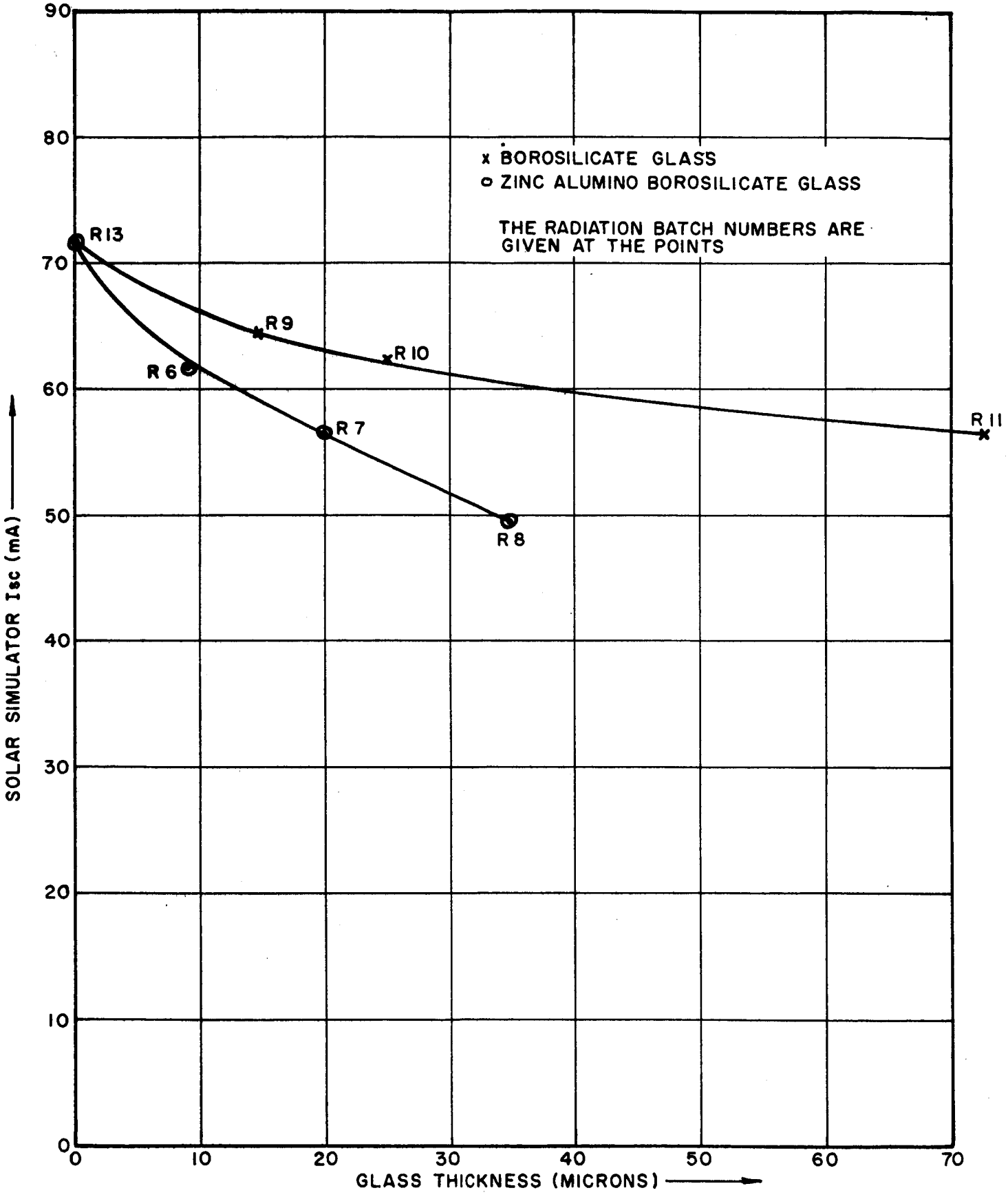


FIGURE 18 - Isc AS A FUNCTION OF BUILT UP THICKNESS OF FUSED LAYERS

Use of High Temperature Contacts to Evaluate the Effects of Glass Fusion

Although at first, solar cell fabrication method (a) described in Section 4.4 was used most, later work used method (c). The high temperature contact structure was used on the front surface of the cell, and in some cases the back contact of titanium-silver was present before glass fusion. These contacts increased in series resistance slowly enough that after fusion, the true I_{sc} could still be measured. As mentioned above, when this was the case, the parameters governing glass fusion could be rapidly assessed from the cell characteristics, thus facilitating the search for optimum fusing conditions.

Another example of the usefulness of these contacts could be seen in the figures below, which show for standard tungsten illumination, the values of I_{sc}, P_{max} and the dark reverse current for a cell coated with borosilicate glass, and then given three additional 5 minute heatings at 735°C.

	I_{sc} (mA)	P_{max} (mW)	I_{rev} at -0.7 V (μA)
Starting cell	60	22	10
Cell + glass (fused 760°C-7 min.)	55.5	20	>500
Re-etched edges	55	19.5	85
Reheated 735°C - 5 min.	52.7	18	95
Reheated 735°C - 5 min.	53	17.5	110
Reheated 735°C - 5 min.	54.5	16.5	140

The steady decrease in P_{max} was caused by increasing series resistance. Later trials showed that much of this degradation could be recovered by removing the back contact, and making a fresh contact on the re-sandblasted surface.

Separate Effects of Heat Treatment and Glass Fusion

Another set of trials compared the performance of cells which had been heated through the fusion cycle, with and without the glass, to the performance of control cells which were not heated. The fusion cycle heated the cells to 890°C, and cooled to near room temperature, all within 30 seconds. Two different cell surface conditions were used. Six cells with a polished front surface, had titanium-silver contacts evaporated over a silicon monoxide layer 750 Å thick. The other six cells had a lapped surface finish, and the titanium-silver was evaporated over a phosphosilicate glass antireflecting film. The back contacts were applied, and the cells were etched. Although the silicon monoxide coating allowed an increase in series resistance, the I_{SC} values could still be compared. The results, averaged for two cell groups, are given in Table 3. The degradations are typical of those observed on the best cells produced in this work, and they are in qualitative agreement with the lifetime degradation observed under similar conditions. The silicon monoxide coated, polished cells had lower I_{SC} values under tungsten, but had comparable values under the simulator. This was also the case for cells without covers and supported the visual impression that the transparency of the fused coatings was good enough to allow the cell coatings to retain the effectiveness they had without covers.

Effect of Fusing Temperature

A good example of the combination of high temperature contacts, and fusion cycles, is given by measurements on three cells, all with a lapped finish with phosphosilicate glass coating. The maximum fusion temperatures were 890°C, 920°C and 950°C for cells 1, 2 and 3 respectively, and in each case the cycle was completed within 30 seconds. Figure 19 shows I-V curves under both tungsten and the solar simulator. The higher fusion temperatures increased I_{SC}, and also decreased the series resistance, which was measured to be 1.4 ohms for cell 1 and 1.2 ohms for both cells 2 and 3.

TABLE 3. Separate Effects of Heat Treatment and Glass Fusion.

Cell Surface Preparation	Treatment	I_{SC} (Tungsten, 100 mW/cm^2)	Degradation From Control	I_{SC} (Solar Simulator, 140 mW/cm^2)	Degradation From Control
Polished + Silicon Monoxide	Control	58.5 mA	--	74.5 mA	--
	Heated	55 mA	6%	70 mA	6%
	Glass Coated	53 mA	9.5%	65 mA	13%
Lapped + Phospho-silicate Glass	Control	61 mA	--	74 mA	--
	Heated	58.5 mA	4%	71 mA	4%
	Glass Coated	55 mA	10%	66 mA	11%

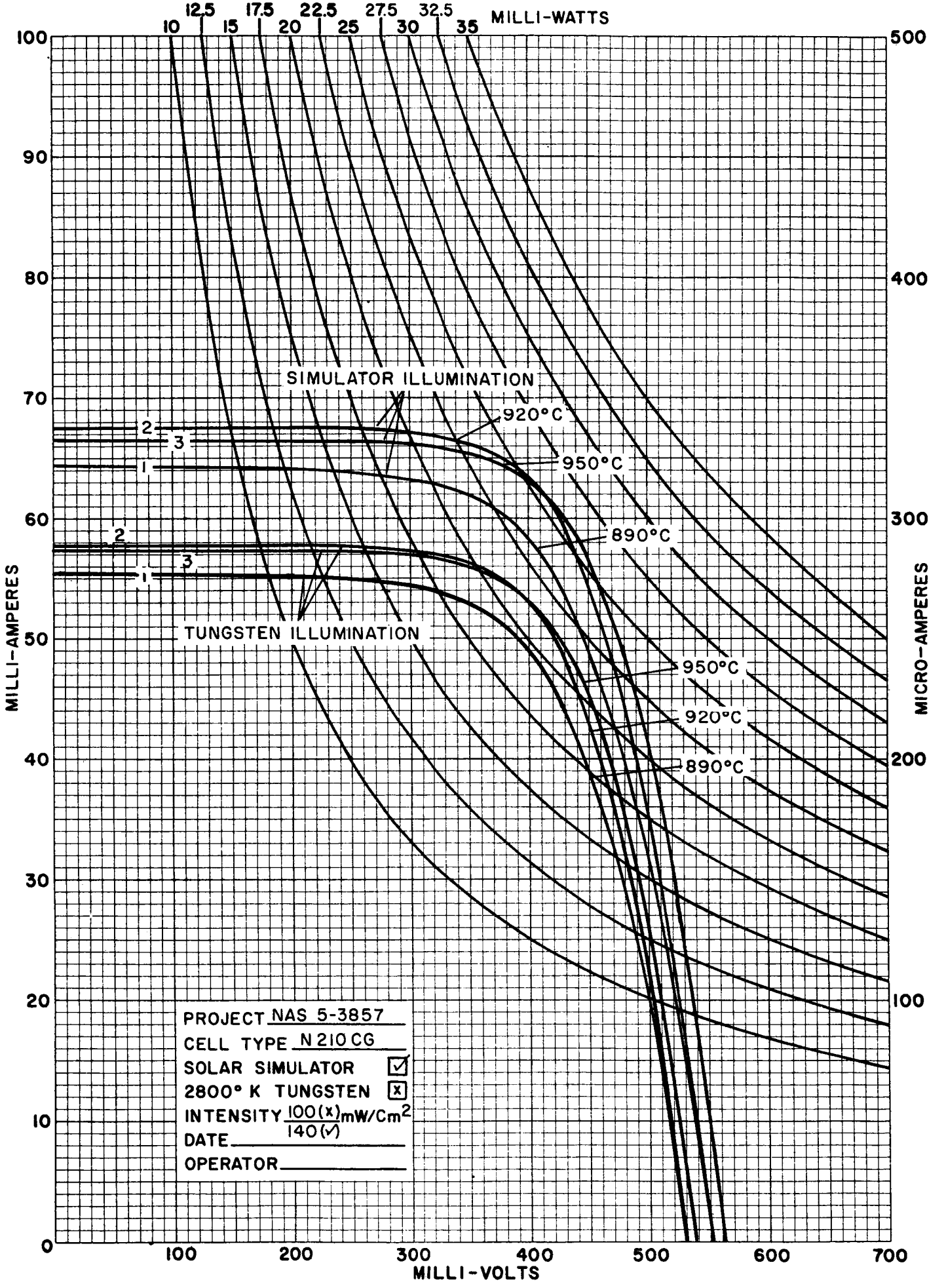


FIGURE 19 – I-V CURVES FOR VARIOUS FUSING TEMPERATURES

Transparency of Fused Glass Layers

In addition to comparisons with control cells, another test of the fused glass layer was possible. In this, the cell was coated with glass and its photovoltaic characteristics measured. Next, the glass layer was dissolved off using hydrofluoric acid, and the cell was coated with a transparent organic material, often the adhesive used to hold glass covers. The refractive indexes of these materials and the glass were almost equal, ensuring identical reflective losses for the two cases. Any increase in current for the adhesive coated cells indicated a lack of transparency in the glass, because the adhesive was known from separate measurements, to have high transmission. Early tests of this type with zinc alumino borosilicate glass showed up to 12% decrease in transparency and this was one strong incentive to seek more transparent glasses. The differences introduced by the borosilicate glass were less than 2%, indicating that the losses caused by fusing layers of these glasses were largely the result of degradation in the cell itself. These results were supported by tests of the output from a fine light spot moved across the cell over regions with and without glass.

Besides spectral transmission tests of slides (see Section 5.6), a quick assessment of the transparency of slices of the glasses used, was obtained by measuring the output of a small area solar cell, first bare, and then covered by the glass slice. In this way, thick slices with polished faces, and thin fused layers which had been removed carefully (see Section 5.2), were measured. Thick samples of zinc alumino borosilicate glass, borosilicate glass, and micro-sheet glass gave insertion losses (under simulator illumination) of 10.5%, 6.5% and 5% respectively.

The reflection losses, estimated from the refractive indexes were 5.3%, 3.6% and 4.5%. This left trans-mission losses of 5%, 3% and 0.5% respectively for the three glasses.

Another test (under tungsten illumination) compared the insertion losses of a thick (20 mil) slide of borosilicate glass with those of a thin (1 mil) fused layer of the same glass. The thin slide was 7% less transparent, and this qualitatively agreed with the decreased I_{SC} values on coated cells.

Wraparound Contacts

One contact configuration used was the "wraparound" type, where the diffused N+ layer was continued around to the bottom of the slice, and the contacts to both N+ and P regions were made on the bottom surface. This allowed the entire top layer to be coated with borosilicate glass. Although the curve shape was not good, the final electrical results were promising. Under tungsten illumination, I_{SC} was 59 mA for the cell before coating, and 55 mA for the coated cell. The P_{max} values were 18.5 mW and 17.5 mW respectively.

Tests with Thick Slides of Glass

Thick (20 mil) slides of borosilicate glass were formed, and were bonded to the cells, either by direct fusion, or by using a thin prefused layer of slurry containing a similar glass. In the former case, the loss in putput was lower, but the adhesion was limited to a few regions of the cover and was largely between the grid lines and cover. The adhesion with the glass "solder", was good.

Typical values of I_{SC} and P_{max} for the two cases under simulator illumination, were 65 mA, 18 mW and 57 mA, 15 mW. The low I_{SC} value for the solder case was not expected. In both instances, some of the power loss was caused by increased series resistance, the result of the longer heating needed for the increased mass of glass involved.

b) Contact Measurements

The evolution of compatible contacts described in Section 4.6 was an important step forward in this work. Here, some of the contact trials are described.

Deep Diffused Regions Under the Top Contacts

Early trials of cells with a junction depth of several microns showed no shorting caused by contact metal penetration during two fusion cycles of 730°C - 5 minutes. This supported the concept of using deep diffused areas under the front contacts. As mentioned, such a structure was made successfully. The process steps were a deep N+ diffusion (2 microns) into P-silicon, masking to cover the required contact area, etching to remove the rest of the N+ layer, re-diffusing to give the usual shallow N+ layer, re-registering evaporated contacts over the deep diffused regions, and coating with glass. The best cells obtained thus, in tungsten, had I_{sc} = 51 mA and P_{max} = 17 mW. The main problems were in the possibility of lowered lifetime because of the double diffusion cycle, and in the re-registration of the grids. However, there is still a need for more work investigating some of the obvious alternate ways to produce this structure.

High Temperature Contacts

The most convenient contact method, as mentioned, was to leave a thin dielectric layer between the titanium and the silicon. Some of the results described in the first part of this section showed that a 750 Å film of silicon monoxide gave fair results, but was not completely satisfactory. With thicker silicon monoxide layers there was less metal penetration, but the antireflecting properties of these films were much inferior to the 750 Å layer.

A hybrid structure illustrating that the glass could be applied to any of the present-day silicon solar cell surfaces, gave good results. Here, in contrast to most slices used, which had a lapped finish, with the

phosphosilicate glass coating, some mechanically polished P-slices were given the usual phosphorus diffusion. The front contacts were evaporated over the phosphosilicate glass, and a mask was applied to cover these contacts. The remaining phosphosilicate glass was removed by hydrofluoric acid, and the cell was coated with 750 Å of silicon monoxide, and a layer of borosilicate glass was fused over the cell. The best electrical results were promising. Under tungsten illumination, I_{sc} = 54 mA, P_{max} = 20 mW. Under simulator illumination I_{sc} increased to 68 mA, again illustrating that the glass layers maintained the full effects of the antireflecting coatings since this enhanced ratio of $\frac{\text{simulator}}{\text{tungsten}}$ current is found also on polished cells with silicon monoxide coatings, with no glass applied.

Measurement of Contact Resistance

Some measurements were made on the high temperature contacts alone. Three configurations were used to measure the contact resistance between the titanium-silver contacts, and either the 10 ohm-cm P-silicon or the diffused N+ - silicon, as a function of repeated heat cycles. P-silicon blanks, 10 ohm-cm resistivity were evaporated on both sides with titanium-silver, which was fired at 610°C.

Also some 1 ohm-cm N-silicon slices were diffused with phosphorus, and divided into two lots. One lot had the phosphosilicate glass removed, the other lot retained this glass. Titanium-silver was evaporated onto both sides and fired at 610°C. All slices were given an edge etch to remove leakage paths, and the total series resistance perpendicular to the large faces of the slices, was measured by plotting I-V curves. Checks of the resistance with the voltage polarity reversed showed no curvature in the I-V curves, suggesting that the contacts were Ohmic, and were symmetrical. This last fact was used to derive the contact resistance for one surface by halving the total resistance measured. The slices were given a series of identical heat treatments (770°C - 7 minutes), and

after each treatment the contact resistance was measured (see Figure 20). Although the individual resistance values were different, the general pattern was similar for each type of contact. For the metal to N+ - contact with the phosphosilicate glass, the resistance decreased after the first heat treatment, and then increased, tending to saturate. For the metal to P-silicon contact the resistance increased rapidly from the first heating cycle, again tending to level out. These measurements confirmed the hypothesis described in Section 4.6 of the mechanism underlying the high temperature front contact. The measurements on the metal to P-silicon supplied good reason why the back contact should not be applied until after the glass was fused. Three other observations were of interest.

First, for the metal to N+ - silicon with the phosphosilicate glass removed, the starting resistance was lower than the resistance of the bulk silicon. Second, it was only when the titanium-silver was in contact with this phosphosilicate glass that the slices showed signs of discoloration probably caused by interaction between the titanium and the diffusion glass. Third, after several heat treatments, when the slices with high resistance were soldered, no appreciable change in resistance was observed, showing that the increased resistance was not caused by poor contact between the measuring probes and the metallized surfaces.

5.6 Particle Irradiation

Using the electron accelerator and facilities at Space Technology Laboratories, two irradiation trials were carried out.

Irradiation of Slides

In the first trial, some transparent slides had their transmission measured using a monochromator, were irradiated with 5×10^{15} 1 Mev electrons per cm^2, and the transmission was measured again. The samples were of four types, 6 mil microsheet (0211 glass) with evaporated filter layers, 30 mil

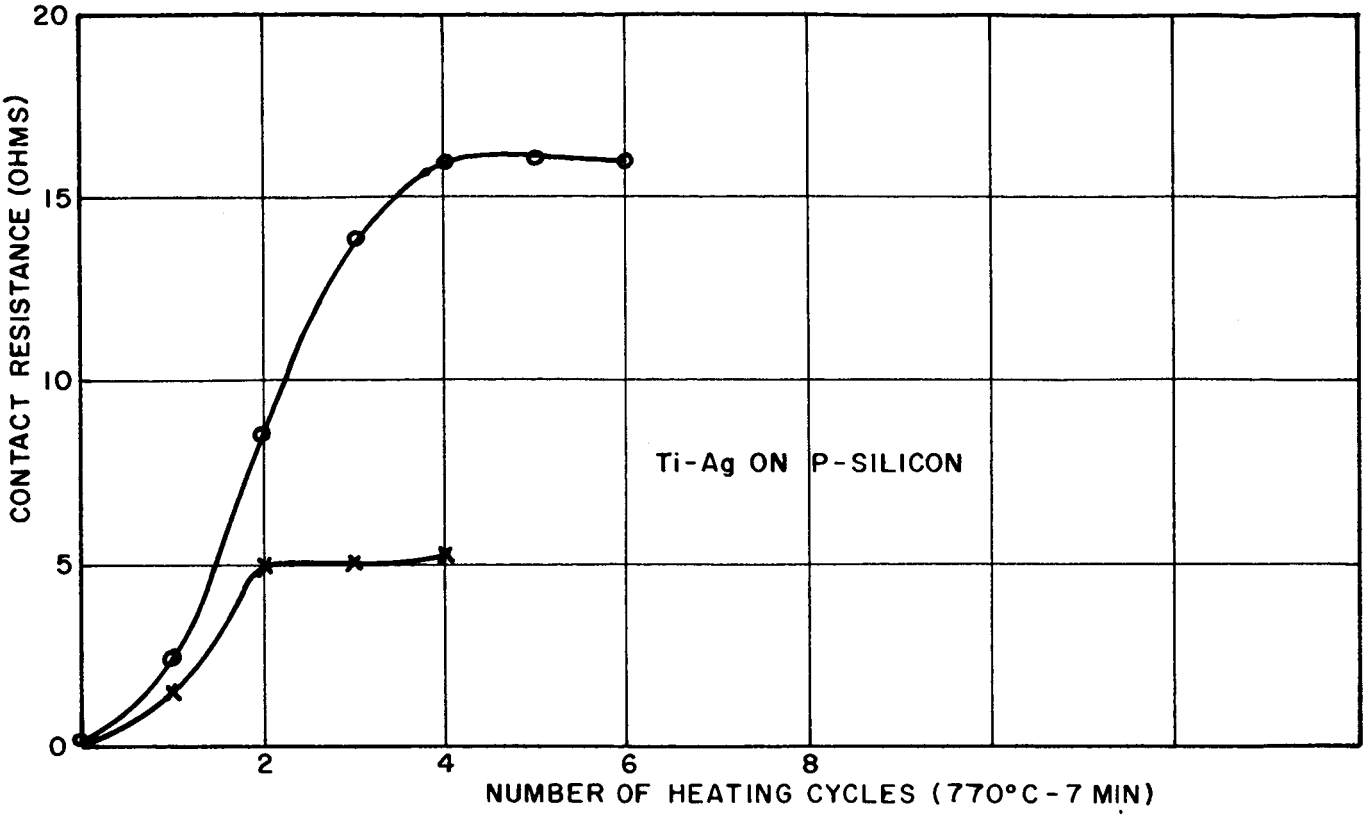


FIGURE 20 (a) - CONTACT RESISTANCE VS. NUMBER OF HEATING CYCLES

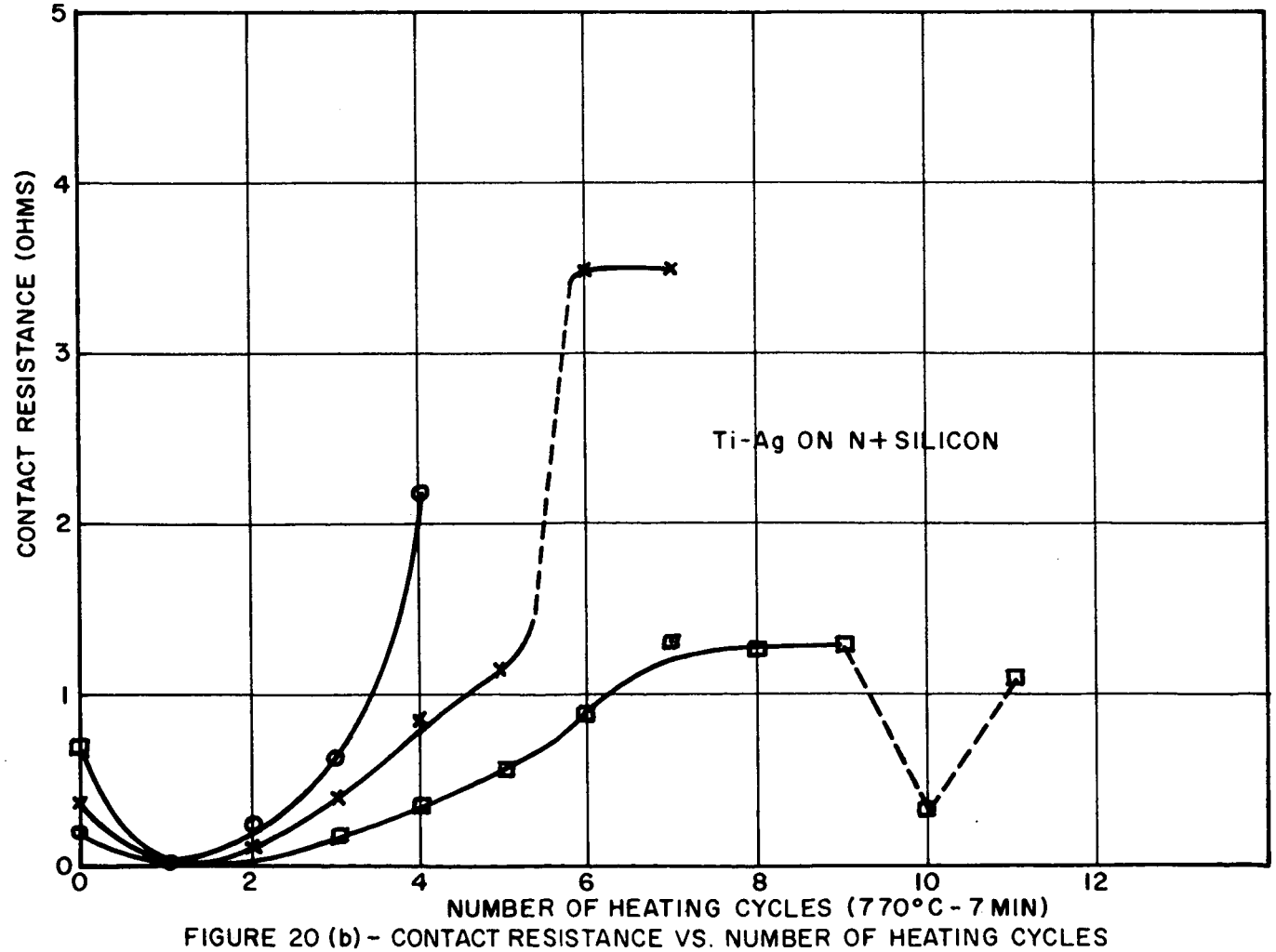


FIGURE 20 (b) - CONTACT RESISTANCE VS. NUMBER OF HEATING CYCLES

clear fused quartz, 30 mil clear fused quartz with a sintered layer 1/2 mil thick of zinc alumino borosilicate glass, and a 13 mil polished slide of this same glass. The results of these measurements are shown in Figure 21. The transmission losses in the first three samples were low (2 to 3%) but the slide of the integral glass degraded considerably (10%). This was another of the reasons for changing to borosilicate glasses.

Irradiation of Cells

The second trial was more comprehensive. It was designed to compare the radiation resistance of several variants of integrally coated cells with that of a number of control batches. The dosage was 2×10^{15} 1 Mev electrons per cm^2, and the cells were split into two groups for separate irradiation. The consistency of the results on the two groups showed that the accelerator dosage was well controlled. The batches of three cells are identified in Table 4. Batches R1 to R5 were controls using the two present-day forms of N/P cells, bare and with conventional cover slides. Batches R6 to R8 and R9 to R11 all had high temperature contacts, and tested the effect of increasing the thickness of zinc alumino borosilicate glass or borosilicate glass respectively. R8 and R11 included samples of matte glass coatings. R12 was a trial of thick borosilicate glass slides, fused direct, or using glass solder. R13 was included to find any reaction between the glass fusion cycle only, and irradiation. R17 was like R13, with a cover slide added. On R14 to R16 the glasses were fused before plated contacts were added. All cells were made with the same diffusion schedule, from P-silicon in the resistivity range 8-12 ohm-cm. During preparation and measurement of the samples the effectiveness of the slurry control, and the conclusions above regarding the similar spectral response with and without glass layers, were confirmed.

Before and after irradiation, I-V curves for all the cells were traced under both simulator and tungsten illumination, and the spectral response of one cell in each batch was measured. There was good consistency of both sets of measurements within each batch. The averaged simulator I_{SC} values are given in Table 5, and also in Figure 22. The

TABLE 4. Particle Irradiation Samples

Group	Cell Surface Finish	Contacts Front	Contacts Back	a/r Coating On Cells	Cover Details
R1	Lapped	Au-Ni	Au-Ni	Ph-g(1)	None
R2	Polished	Ti-Ag	Ti-Ag	SiO	None
R3	Lapped	Au-Ni	Au-Ni	Ph-g	6 mil 0211(7)
R4	Polished	Ti-Ag	Ti-Ag	SiO	6 mil 0211(7)
R5	Polished	Ti-Ag	Ti-Ag	SiO	20 mil quartz(2)(7)
R6	Lapped	High Temp	Ti-Ag	Ph-g	9 microns IG-1(3)
R7	Lapped	High Temp	Ti-Ag	Ph-g	20 microns IG-1
R8	Lapped	High Temp	Ti-Ag	Ph-g	35 microns IG-1
R9	Lapped	High Temp	Ti-Ag	Ph-g	14.5 microns IG-2(4)
R10	Lapped	High Temp	Ti-Ag	Ph-g	25 microns IG-2
R11	Lapped	High Temp	Ti-Ag	Ph-g	73 microns IG-2
R12	Lapped	High Temp	Ti-Ag	Ph-g	20 mils IG-2
R13	Lapped	High Temp	Ti-Ag	Ph-g	None(5)
R14	Lapped	Au-Ni	Au-Ni	Ph-g	16 microns IG-1(6)
R15	Lapped	Au-Ni	Au-Ni	Ph-g	14 microns IG-2(6)
R16	Lapped	Au-Ni	Au-Ni	Ph-g	38 microns IG-2(6)
R17	Lapped	High Temp	Ti-Ag	Ph-g	6 mil 0211(5)

Notes:
(1) Ph-g refers to phosphosilicate glass.
(2) Incomplete cover, bare areas .05 cm^2 along each long edge.
(3) IG-1 was zinc alumino borosilicate glass.
(4) IG-2 was borosilicate glass.
(5) Taken through fusion cycle.
(6) Contacts plated through etched slots.
(7) The filters used were OCL1 207 SCC 400-2, with 400 millimicron cut-off, and antireflective coatings.

TABLE 5. Values of I_{SC} Before and After Electron Irradiation.

Radiation Batch	I_{SC}, Solar Simulator (mA) Before	After	% Decrease
R1	70.8	56.7	20
R2	71.3	56.3	21
R3	69.8	54.4	22
R4	70.7	52.5	25.5
R5	71.0	56	21
R6	61.7	49.9	19
R7	56.6	46	19
R8	49.6	39.7	20
R9	64.4	52.8	18
R10	62.4	51.5	17.5
R11	56.9	45.7	19.5
R12	56	43.1	23
R13	71.7	59.1	17.5
R14	54.6	44.7	18
R15	59.6	48.6	18.5
R16	57.2	45.5	20.5
R17	71	55.4	22

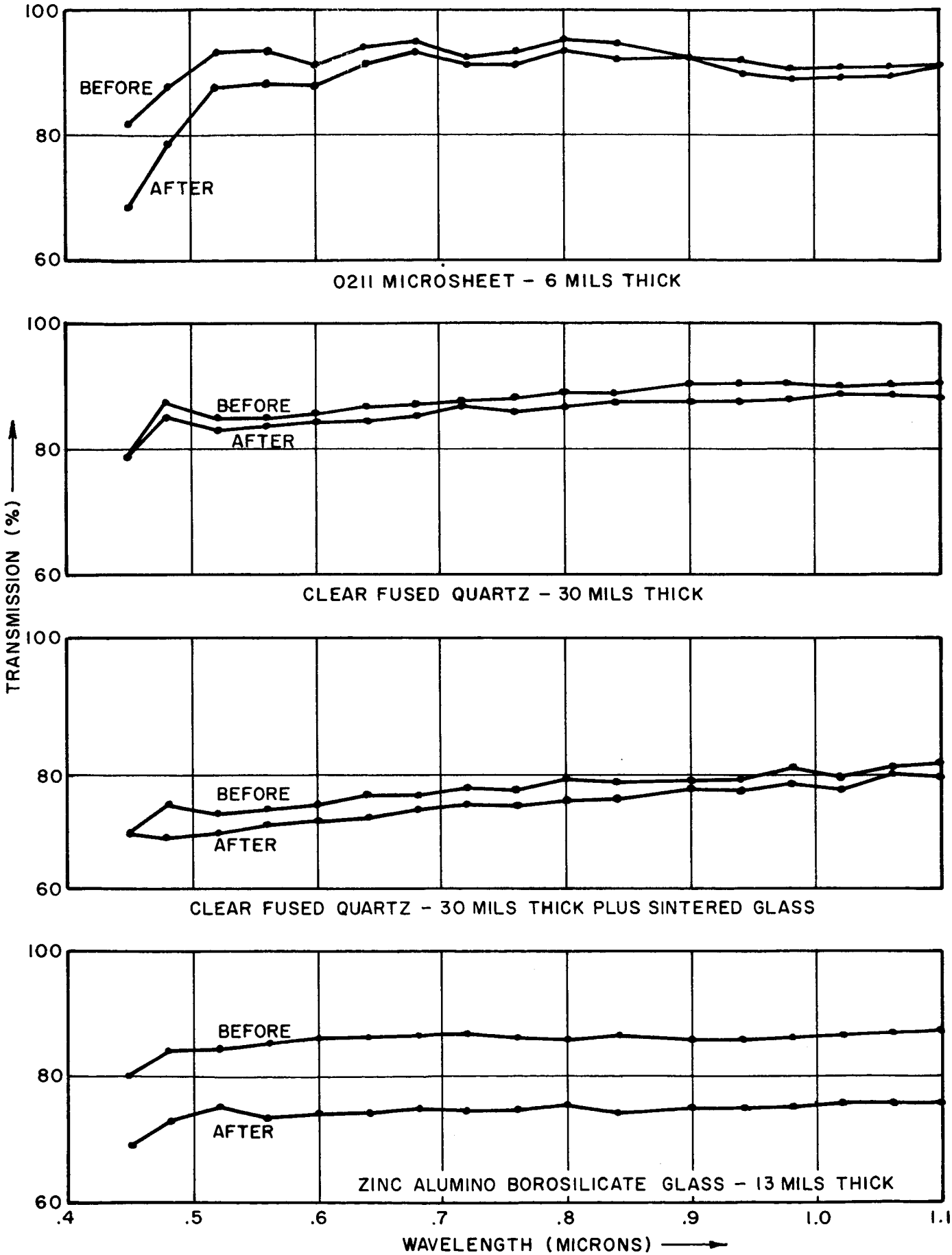


FIGURE 21 - TRANSMISSION VS. WAVELENGTH FOR VARIOUS SLIDES

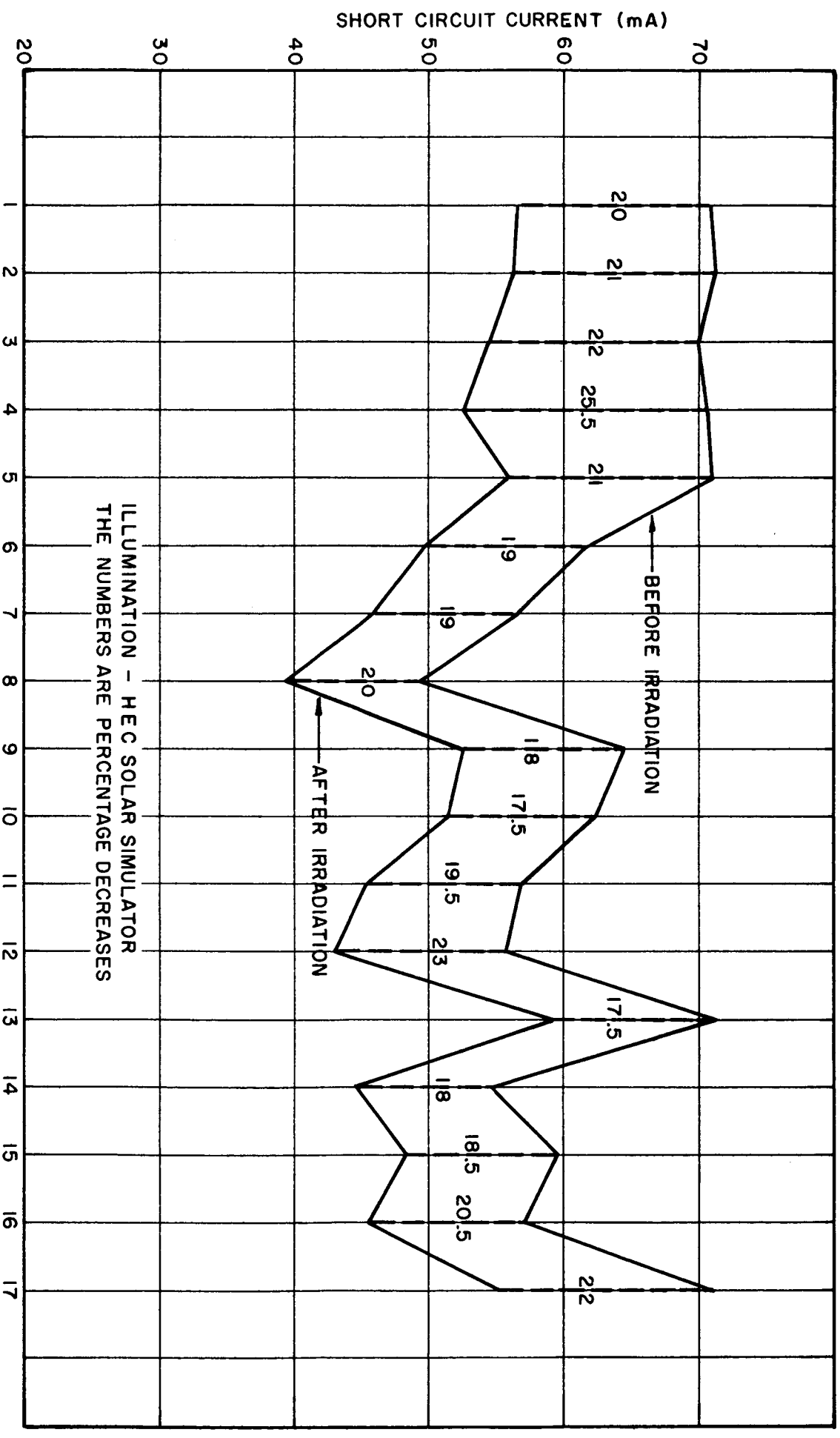


FIGURE 22 - I_{sc} VALUES FOR RADIATION BATCHES, BEFORE AND AFTER IRRADIATION

changes in relative response followed a similar pattern, indicated in Figure 23, and the values of response at the four points shown are listed in Table 6.

The conclusion from this trial was that the degradation during irradiation was very similar for all batches, and therefore there was no apparent correlation between the radiation resistance and cover thickness

Anomalous I-V Curves

Some interesting post-irradiation tests arose from the observation that after irradiation, the I-V curves in some of the batches had a change of curvature towards the V_{OC} region. The batches showing the effect were R6 to R13 and R17, although not all cells in these batches showed the same degree of curvature. Examples of the worse cases are seen in curve (2) in Figures 24 and 25. Curve (2) in Figure 26 is typical of the curves for cells not showing these unusual curves. The only common link in cells exhibiting this effect was the same combination of contacts, namely high temperature contacts on the front, and the usual titanium-silver contacts on the back, both contacts being present while the cells were heated through the fusing cycle. During this cycle, the glass was not always present (eg. for R13 and R17) and in addition the integral glasses could not be blamed because batches R14 to R16 had these glasses but did not have anomalous curves. Shelf-aging was eliminated as a cause since similar cells made at the same time, but not irradiated, did not show such curves.

The usual post-irradiation curve was recovered when the back contacts of the anomalous batches were removed (they were found to have very low adhesion), and were replaced by plated contacts (see Figure 24). The slight reduction in I_{SC} was expected from the decreased area after re-etching. If the back contact was replaced by titanium-silver contacts, evaporated and fired, not only was the anomalous curve shape corrected, but also the cell recovered almost to its pre-irradiation level (Figure 25). A conventional irradiated cell (Batch R2) with no contact change was fired at 605°C for 5 minutes, and also showed almost complete recovery (Figure 26).

TABLE 6. Values of Relative Response at Two Wavelengths for Radiation Batches

Radiation Batch	Percentage At 0.5 micron B	A	Percentage At 1.0 micron B'	A'
R1	43	57	79	33
R2	51	63	90	29
R3	46	57	82	36
R4	47	60	81	24
R5	47	62	81	29
R6	36	46	84	40
R7	34	47	85	40
R8	29	39	85	40
R9	38	48	81	36
R10	36	50	80	36
R11	35	45	82	37
R13	41	53	80	36
R14	38	48	83	38
R15	42	54	85	33
R16	37	48	82	36
R17	40	48	78	36

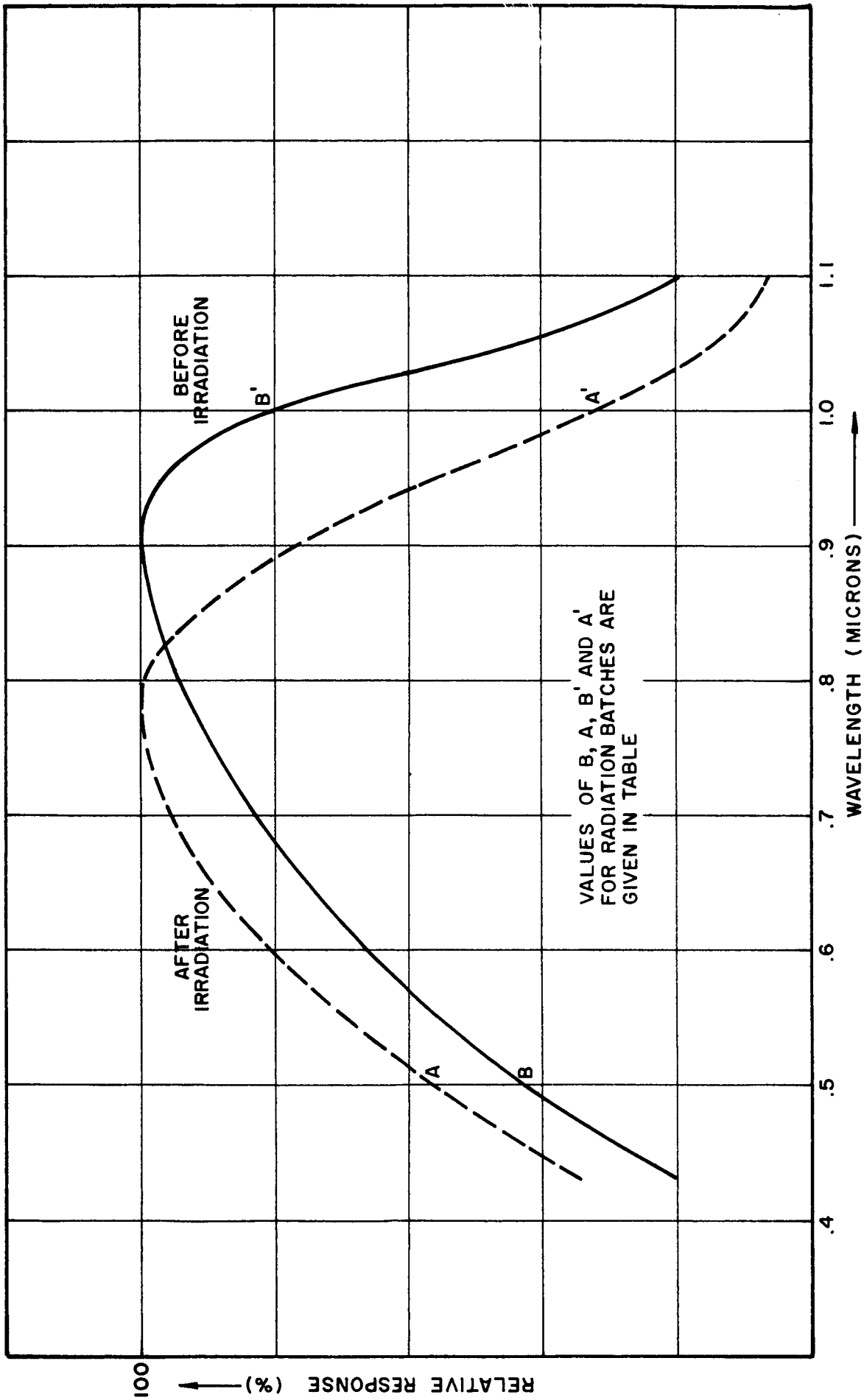


FIGURE 23 – TYPICAL SPECTRAL RESPONSE CURVES

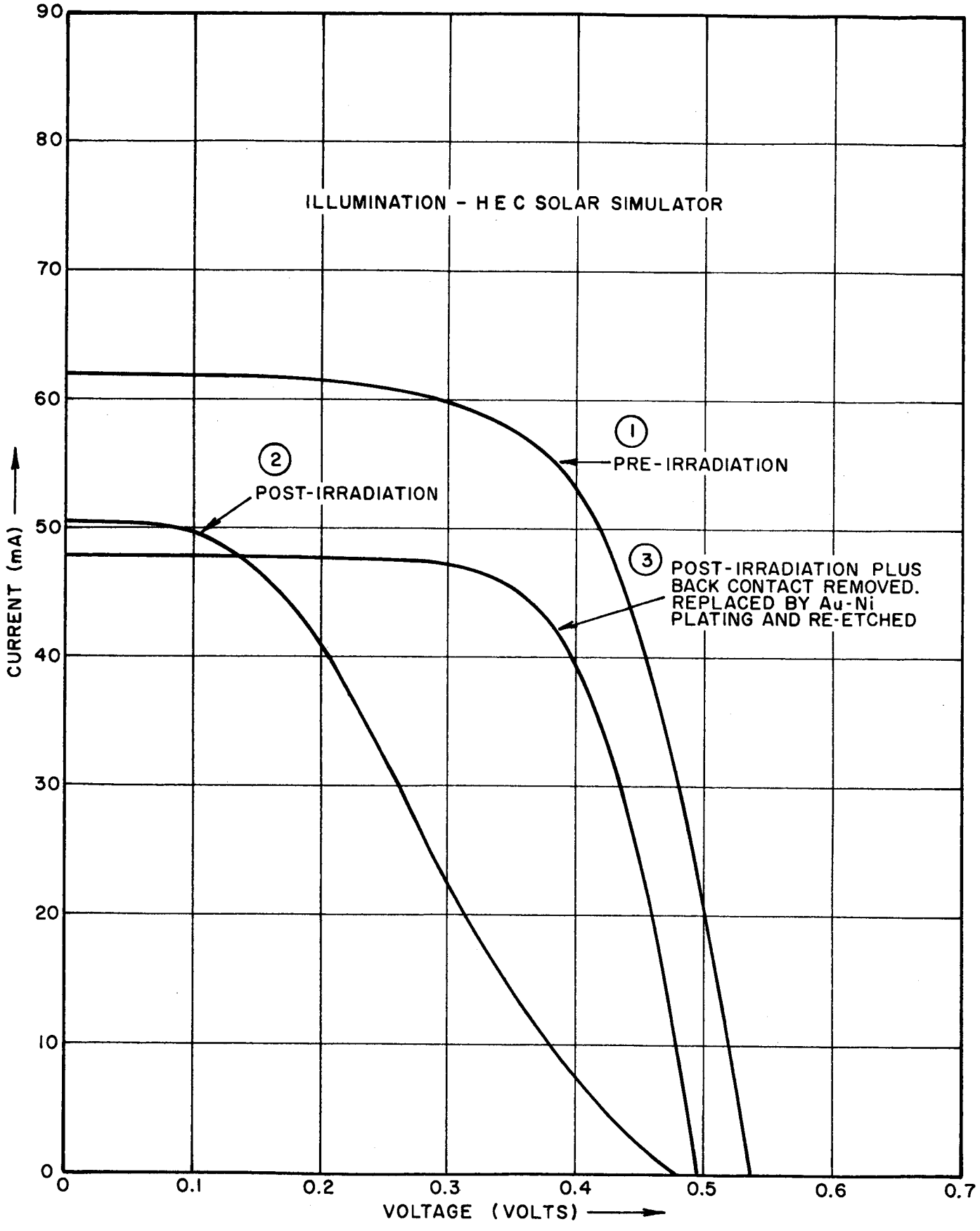


FIGURE 24 - I-V CURVES FOR BATCH R-10

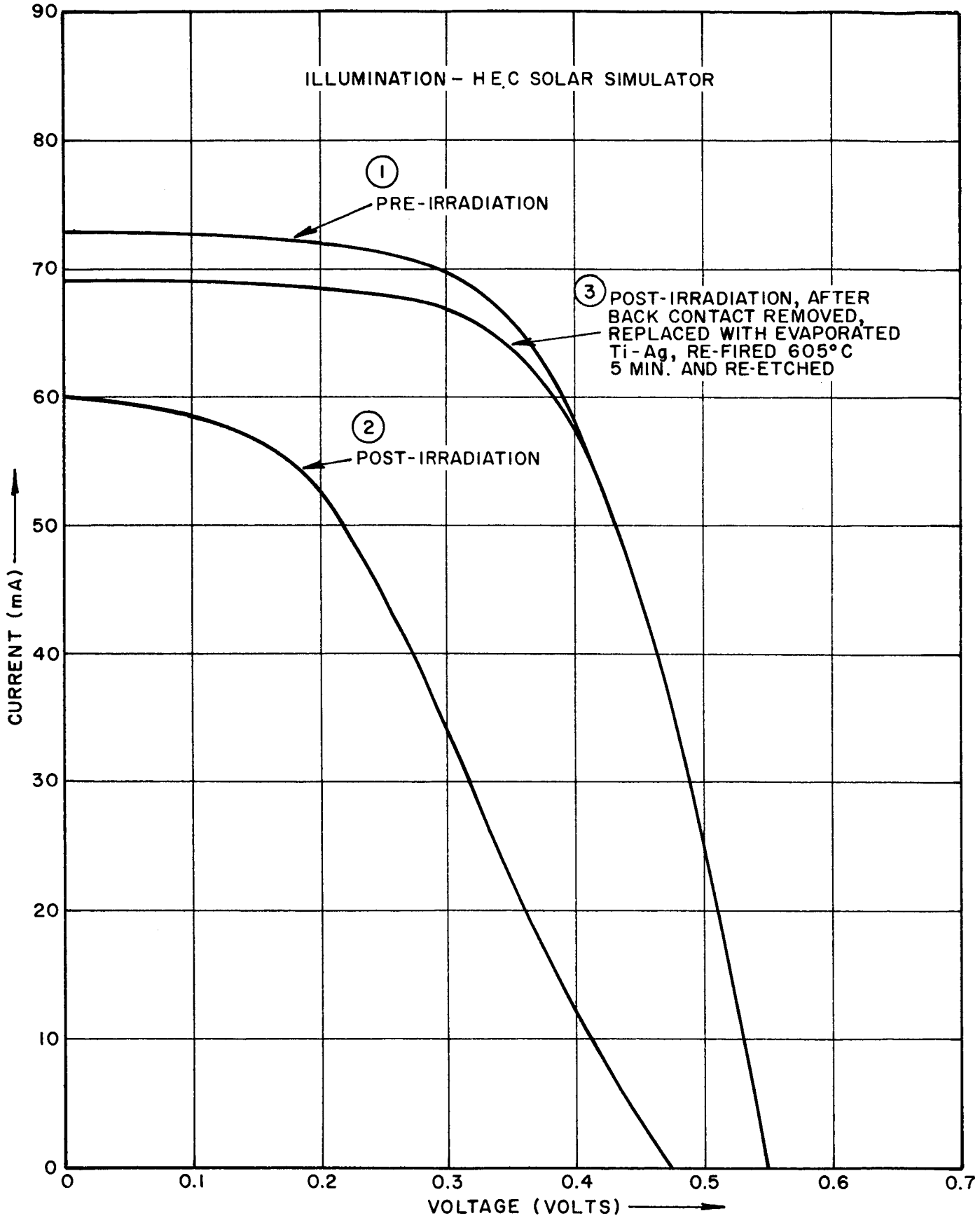


FIGURE 25 – I-V CURVES FOR BATCH R-13

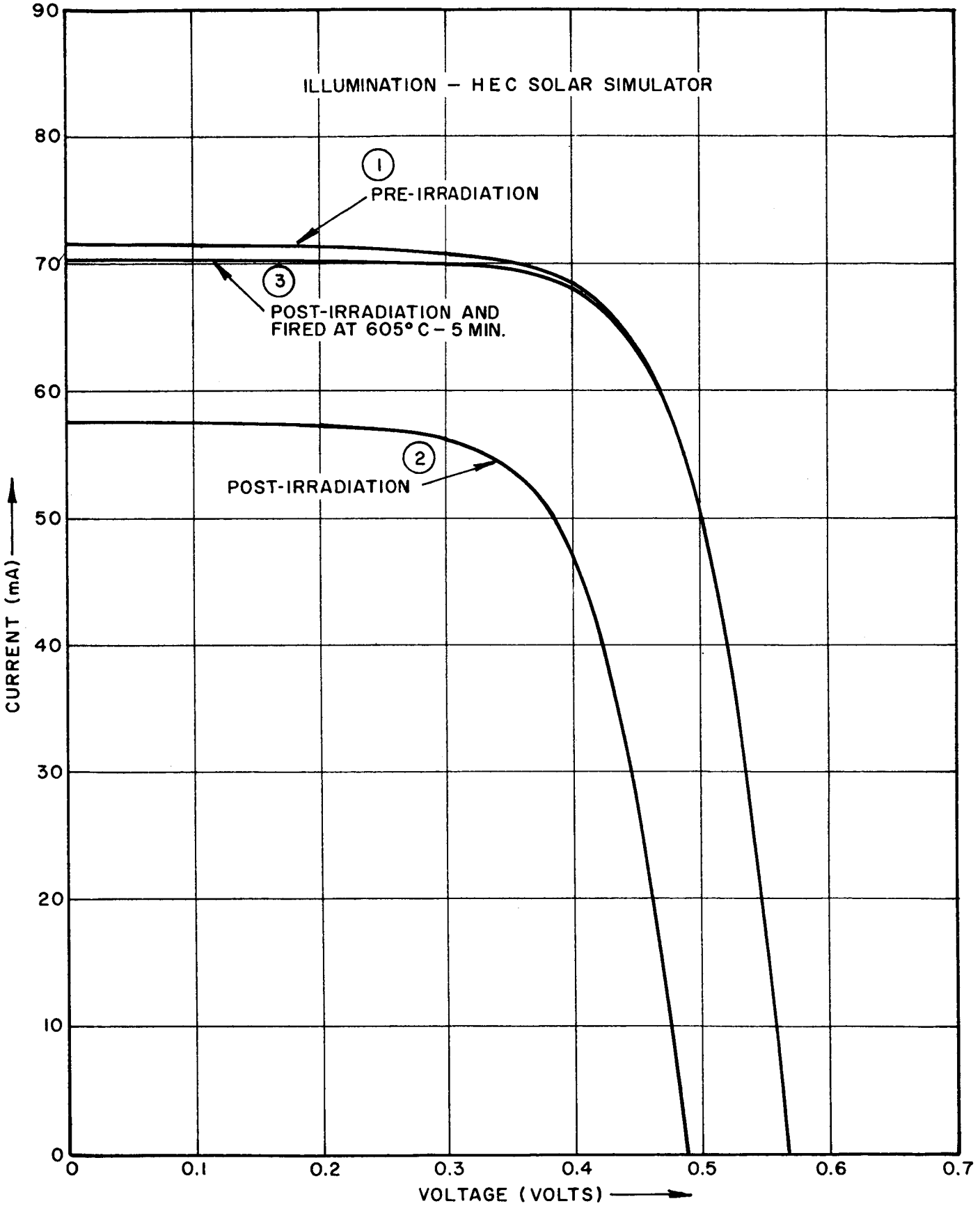


FIGURE 26 – I-V CURVES FOR BATCH R-2

In later work the back contact was applied after glass fusion, and batches R3 to R5 which had this type of contact did not show these effects. Therefore the unusual post irradiation I-V curves could be avoided by changing the back contact. However, although these curves could be avoided, the question remained as to their cause during irradiation. If spike heating was postulated, it is hard to see why some of the other batches, particularly those containing plated cells, did not also deteriorate in curve shape.

It is of interest that with titanium-silver contacts, the irradiation degradation could be recovered by a single firing at 605°C for 5 minutes. This type of contact has added versatility to damage-annealing studies. If annealing of highly damaged cells should be required, the front contacts developed in this work should allow the use of more severe annealing cycles.

In summary, although the bare cells compared better than expected, at least the integral glass coatings did not introduce any adverse irradiation degration. In future studies, for reasons given below in Section 7, the emphasis should be on the protection given by these coatings against damage by low energy protons.

5.7 State Of Art Samples

Towards the end of the contract, 100 cells made with the best state of art were delivered to NASA. The details agreed on for their fabrication now follow. The cells were made from lapped and lightly etched P-silicon, 8-12 ohm cm, with a phosphorus diffused layer 0.3 microns deep. The phosphosilicate glass was left in place and titanium-silver contacts were made to the front surface. Borosilicate glass of thickness 25 microns, with deviations specified to be less than ± 5 microns if possible, was fused to the cells. The back surface was then sandblasted, a titanium-silver contact was evaporated and fired-in, and the cells were etched.

Approximately 150 slices were processed, and the yield obtained was very satisfactory, 90% being above 8.5% AMO* and 65% were above 9.5% AMO. The 100 cells submitted were chosen for good over-all appearance and complete glass coverage, and with good electrical characteristics. Of these submitted cells, 75 were above 9.5% AMO, and the measured spread of the I-V curves of this 75% is given in Figure 27. The simulator I_{SC} values were greater than 64 mA for 90 of the cells submitted, and ranged up to 69 mA. The typical value of series resistance was 1.4 ohms ± 0.2 ohms, compared to 0.9 ± 0.2 ohms for control cells made in the conventional way. This increased series resistance accounted for some of the loss of power output, but as mentioned above, improved front contact design should increase the output power. On each tenth cell in the 100 final samples, the glass thickness was measured, and the measurements are shown in Figure 28. The thickness control is seen to be well within the target spread.

Figure 29 shows a cell like those used for the state of art samples. In this case, only the cell to the left of the arrows was covered with glass, and on this side the good transparency, and some of the drying patterns can be seen. The glass layer stopped short of the edge contact (like the sample shown in Figure 11(b), but in practice, the glass layer could be continued up to this contact.

* This means the cell had conversion efficiency = 8.5% under simulated sunlight, air mass zero.

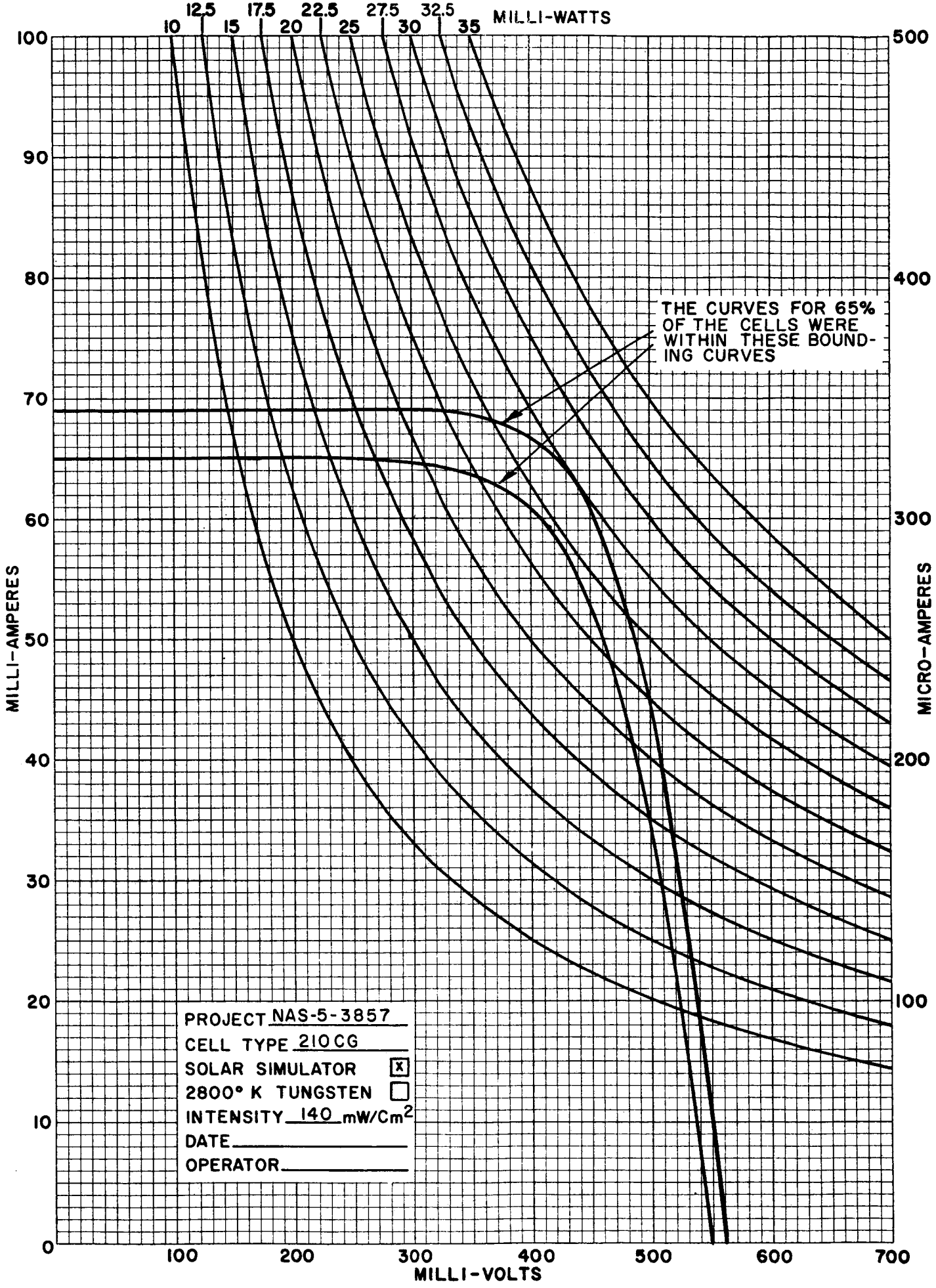


FIGURE 27 - I-V CURVES FOR STATE OF THE ART SAMPLES

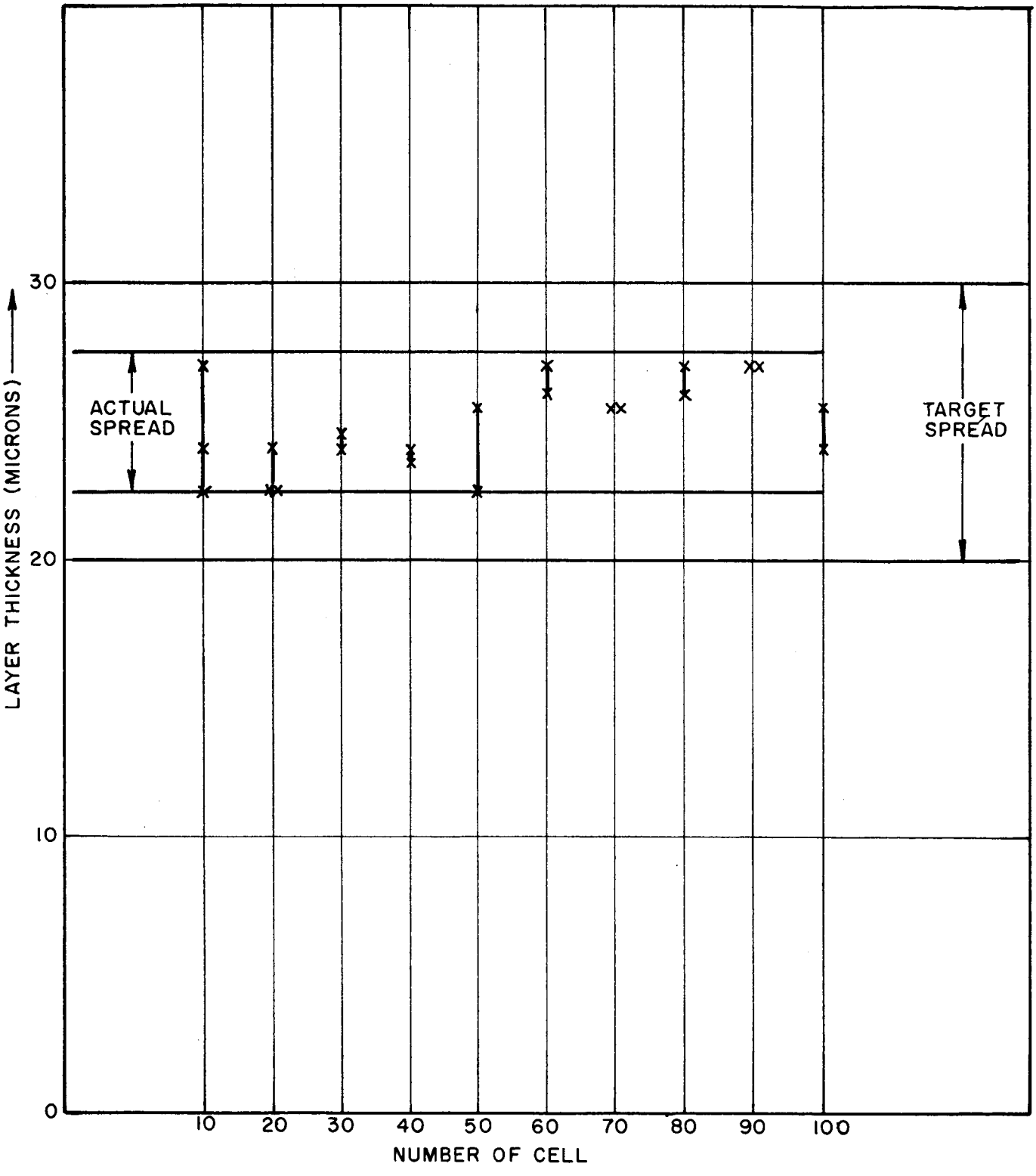


FIGURE 28 – THICKNESS OF GLASS LAYERS ON 10 STATE OF THE ART SAMPLES

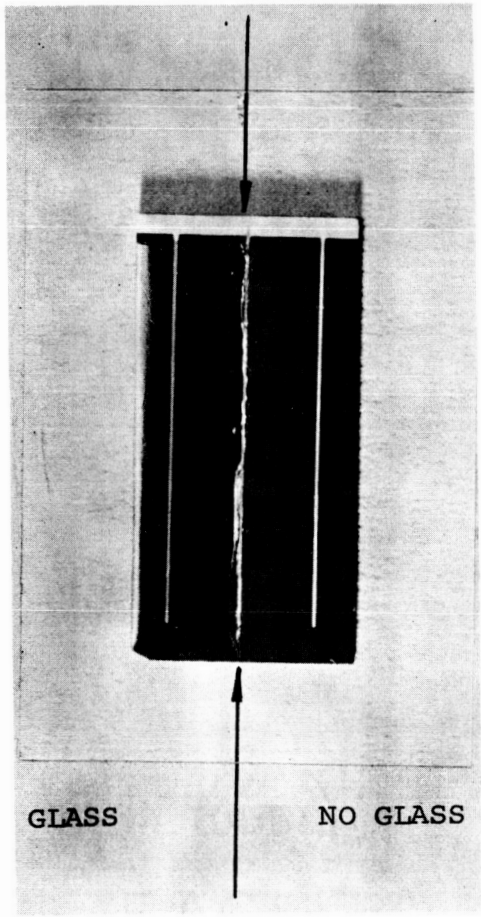


FIGURE 29 - SOLAR CELL PARTLY COVERED WITH INTEGRAL GLASS.

6. ASSOCIATED TOPICS

Alternative Glass Application Methods

Two methods, other than the centrifuge method described above, were tried for depositing glass powder onto slices. The first method sprayed slurry over the slices using an air gun. In this way fair glazed slices were obtained but there was much glass powder wasted, and also the force of the stream of slurry dislodged glass powder already in place on the slice. In the second method, a high electric field was applied between the slice and a metal electrode, both immersed in a slurry. Potentials up to 3 KV were used but no noticeable electrophoretic action resulted.

Trials For Thicker Layers

Early in the contract, attempts were made to build up thick layers (~ 5 mils) in one application of a dense slurry. The problem was that the resultant glass layer contained mostly bubbles and even the use of very high fusing temperatures did not improve the transparency. Attempts were also made to fuse the glass layer in a vacuum, after preliminary pump-down and baking. It was hoped that this procedure would de-gas the slurry and remove the bubbles, but these layers were still unsatisfactory. Later work which enabled thicker preformed slides to be applied, lessened the need for applying thick fused layers.

Formation Of Thick Glass Slices

A few trials were made to withdraw thick slices from molten glass matched to silicon. These tests were not successful, but it was known that the crucible used was not suitable. When such slices were usable, following development of the compatible contacts, a commercial vendor was found who would produce sample quantities of such slides. Should these slides become necessary in future work, the quality of these commercial slides can be improved, and some alternative methods for forming slides are available for investigation.

Flame Fusion

Several attempts were made to improve the quality of the glass layers by flame fusion. This method has the merit of heating the glass layer direct, minimizing extreme heat cycling of the cell. Along the same lines, some tests were done where the slice was mounted glass side down on the heater strip, with a suitable layer not wetted by the glass between the sample and the heater. Neither method improved the layer qualities.

Antireflecting Films

Some increased output should be possible by reducing the reflectivity of the fused glass layers. The matte surface mentioned above was one means of doing this. A suitable dielectric layer could also suffice. For glasses with refractive index in the range 1.5 to 1.6, the refractive index of the dielectric should be 1.3 or less. A possible solid was magnesium fluoride, but time did not permit a trial. However, some liquids (methyl alcohol, water) have suitably low refractive index, but when they were applied to some glass covered cells, no appreciable improvement was observed. The theoretical decrease in reflectivity is from 4% to 2%, and based on this, it is felt that a slightly increased output would result from application of a suitable dielectric layer.

Environmental Effects

Because of the high fusion temperatures, the glass layers and the cells are stable under the normal high temperature tests required for solar cells. Prolonged heating at temperatures above 600°C should be possible by slight modification of the present cell contact structure.

Some temperature shock trials, where glass covered cells were transferred quickly between boiling water and liquid nitrogen, did not remove the layer, and did not degrade the cell electrical characteristics. Boiling some coated cells in water for 1 hour did not produce electrical or visual changes.

Scaling-Up

The experience gained showed there was good possibility of scaling-up to higher production rates. The fabrication of cell blanks up to the application of glass powder, and the steps following fusion, are minor modifications of already established production methods for solar cells. The fusion is capable of being speeded up by use of a larger strip heater, or by moving the slices continuously through a suitable temperature gradient. The major problem is in the production of the glass powder. Some trials with larger grinding mills were promising but were still slow. Estimates of the slurry usage were possible using the work to date. As an example, consider a slurry giving 1 mil of borosilicate glass. By Figure 5(b), this corresponds to a slurry of density 4.4 mg/ml. Assuming 20 ml of slurry 1.8 cm high, each cell should receive 16 mg. The calculated mass for 1 mil of borosilicate glass was 10.6 mg. This shows over 50% usage, the rest being accounted for by losses during centrifuging and while the slices were being withdrawn. Assuming close packing of cells, it should be possible to deposit 1 mil layers on 5 cells per batch of 20 ml of slurry, and with 10 batches, 50 cells could be covered. Thus since 15 gm of glass was used to make 200 ml of slurry, the total glass usage is $\frac{0.500}{15} = 3.3\%$. Other tests showed that the glass could be reground and used again, and it should be possible to get 10% usage in this way. Therefore to coat 500 cells per day would only require approximately 50 gm of glass.

Before scaling-up, some of the other methods of application, such as spraying of the slurry would require careful evaluation. Thus although no real attempts were made in this work to scale-up, the figures given show the high feasibility of achieving normal production rates.

7. SURVEY OF CONTRACT, AND CONCLUSIONS

Survey

During this contract the techniques of fabricating silicon solar cells with integral coatings have been extended to provide a quantitative basis for evaluation. Good control of glass slurries was achieved, and fused layers as thick as 6 mils, were successfully applied. Using glass layers as solder, glass covers 20 mils or greater could be applied. Most of the work was concentrated on layers between 1 and 2 mils.

Several commercial borosilicate glasses were found to be superior to special glasses used earlier in this work. Novel contact structures allowed application of glass layers over already-formed contacts, and high quality glass layers were formed. The conversion efficiency of the cells has exceeded 10% AMO, and the cell properties were very consistent. The thermal emittance of cells coated with 1 mil or more of glass approached the emittance of bulk glass. The resistance to 1 mev electron damage provided by the glass coatings was not increased over control cells, although neither was it decreased. The results obtained showed that the processes could be used on a large scale.

Conclusions

Present cover methods fail for slides thinner than 3 mils. The integral coatings show promise for thermal control of solar cells in space missions where high radiation resistance is not required and thin slides are worth using to reduce weight. Such missions include deep space probes, lunar orbiting satellites, and earth satellites operating at low altitudes. The coatings should protect against low energy protons, and may be useful for orbits approaching the sun, where high temperatures must be tolerated. Layers 1 mil thick have one-seventh the weight of present 6 mil covers and the adhesive, and because the adhesive has been eliminated, the reliability of the cell arrays should be greater. With present substrates and cells, the weight saved is around 4.5 pounds per KW. Greater fractional

weight savings are possible if these coatings are combined with light weight substrates and/or lighter cells. The techniques developed should be applicable to thin film cells made from gallium arsenide or silicon, and the coatings are fairly flexible. It is possible if necessary, to coat the edges of cells with glass. Appreciable cost savings are possible, because the expensive optical filters are not necessary, and the complexity of array assembly should be reduced with these coated cells.

The contacts developed in this work show promise for wider use where high temperatures are needed in semiconductor technology. Some of the methods used could be adapted for detailed study of the glass sintering process, or for use in microcircuit encapsulation.

Possible Future Work

Several aspects of the work merit further study.

There is need for further evaluation of glasses. The best glass, not yet found, would be able to form good fused layers directly over the usual production cells. Study of the interaction between some of the glasses and the thin antireflecting coatings used on cells could help to find the cell coating and finish best suited to the glass layer. The use of higher melting point metals in the front contacts would allow higher fusing temperatures. This might improve the glass quality, the limit being set by increased degradation of cell properties.

The front contact design can be optimized closely for specific fusing cycles. Other dielectric layers should be investigated, preferably leading to one that could be deposited immediately before the metal contacts, through the same mask. The structure using a deeper PN junction under the front contacts, showed promise for further study.

Tests are needed of the ability of the glass layers to withstand low energy proton damage and space ultraviolet degradation. There is chance of combining the high temperature contacts with suitable connecting bonds, to allow continuous coatings over interconnected cell arrays. Also wraparound

structures which allow the whole front surface to be glass coated, should be developed further to receive these coatings.

If light weight mounting surfaces or thin cells are available, the use of integral coatings with these should be investigated. Some scaling-up to assess any production problems is justified by results to date.

8. NEW TECHNOLOGY*

Some of the work carried out under this contract may be classified as "New Technology". Description of the first three topics appeared above; the fourth topic is an extension suggested by results obtained. The topics were:

a) High Temperature Contacts.

Metal-semiconductor contacts able to withstand severe heat cycles were developed. Besides use in the present contract, these contacts may be more generally useful in semiconductor work, particularly in annealing studies ion-drift, and other high temperature studies.

b) Contacting Methods.

It was possible to facilitate contact formation subsequent to fusion of integral glass coatings, by removing the deposited glass powder where required by masking, scribing, scraping or by vacuum-suction. This technique too, has possible uses in the wider semiconductor field.

c) Formation of Thin Glass Slides.

After fusing glass powder on silicon or metal, it was possible to remove the unsupported fused glass slide. The layers formed were around 1 mil, but extension to thicker or thinner layers is feasible.

d) Concentrator Design.

Coating a metal concentrator surface with a fused glass layer, should provide a concentrator of high emittance, high reflectivity, light weight, and some flexibility.

* Patent disclosures for material described in this section are being submitted separately to the Office of Patent Counsel, Goddard Space Flight Center.

9. REFERENCES

1. J. M. Palmer "Thermal Characteristics of Solar Cells in Space", Internal Report, Hoffman Electronics Corp. 1963.

2. J. Mandelkorn et. al. "Fabrication and Characteristics of Phosphorus - Diffused Silicon Solar Cells", J. Electrochem. Soc., Vol. 109, p. 313, April, 1962.

3. J. Mandelkorn, "Effect of Impurities on Radiation Damage of Silicon Solar Cells", Paper A-6 in Proceedings of the Fourth Photovoltaic Specialists Conference, Vol. I, August, 1964.

4. R. C. Waddel, "Radiation Damage to Solar Cells on Relay I and Relay II", Paper A-1 in Proceedings of the Fourth Photovoltaic Specialists Conference, Vol. I, August, 1964.

5. K. D. Smith et. al., "The Solar Cells and Their Mounting", Bell Syst. Tech. J., Vol. XLII, p. 1765, July, 1963.

6. F. J. Campbell, "Effects of Radiation on Transmittance of Glasses and Adhesives", Proceedings of 17th Annual Power Sources Conference, 1963.

7. W. A. Pliskin, E. E. Conrad, "Techniques for Obtaining Uniform Thin Glass Films on Substrates", I.B.M. Technical Report TR 22.092.

8. R. Gardon, "Emission of Radiation by Transparent Materials", in "Radiative Transfer from Solid Materials", MacMillan, 1962.

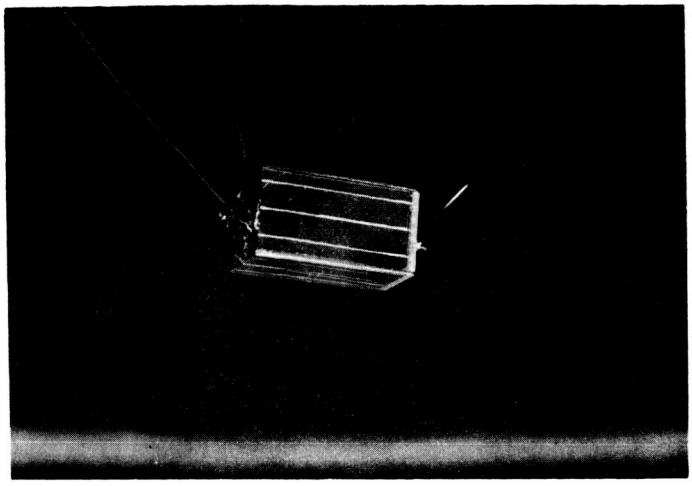
APPENDIX I*

Total Hemispherical Emittance Measurements

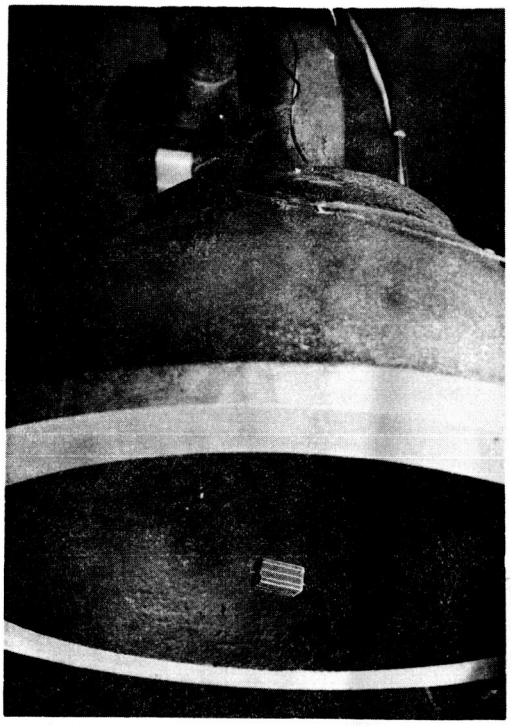
The method used was a calorimetric determination of the heat transfer between the sample and a known environment. A radiative balance was established between the sample, which was maintained at temperature T_S and the surrounding space which was maintained at temperature T_C where $T_S > T_C$. When equilibrium existed between the sample and its surroundings, measurement of T_S and T_C, and of the power required to maintain T_S constant, allowed calculation of the total hemispherical emittance from the Stefan - Boltzmann law.

Four identical solar cells (or slides) were attached by a conductive adhesive to the large faces of a 1 x 1 x 2 cm brass block (see Figure I-1(a). The power was supplied to the block by passing current through a resistor, 100 ohms, 3 watt, ± 1%, fitted into a hole drilled through the block. The power lead-in wires which also supported the block were of 5.7 mil diameter nickel. Nickel was chosen because its Lorentz Number (the ratio of thermal to electrical conductivity) is lowest among common materials. A copper-constantan thermocouple (1 mil wires), soldered to the contact of one of the cells on the block, measured the sample temperature. The heat conduction losses were calculated for these wires. Under the conditions used, the power conducted away was $1.44 \times 10^{-5} (T_S - T_C)$ watts. The effects of conductivity losses through the air were minimized by placing the sample in a vacuum chamber capable of operating below 5×10^{-4} torr. This chamber consisted of two 30 cm diameter cast aluminum hemispheres painted flat black on the inside. The sample block was supported at the center of the sphere formed when these hemispheres were sealed by a neoprene gasket around the equator. Figure I-1(b) shows the supported sample, and Figure I-1(c) shows the hemispheres before closing. The power lost into the vacuum was $= k_1 p(T_S - T_C)$ where k_1 was a complex function of sample and chamber areas, accommodation coefficients, specific heats, molecular weight, and vacuum gauge temperature. When p the pressure was expressed in

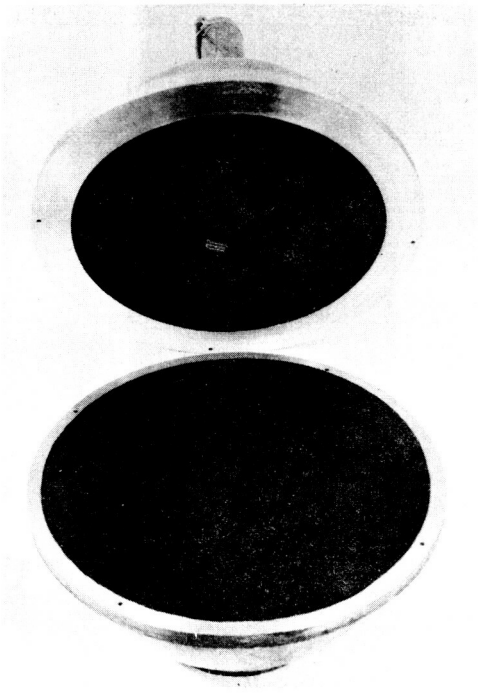
* J. M. Palmer and D. Bickler built and operated the emittance equipment, and wrote this appendix.



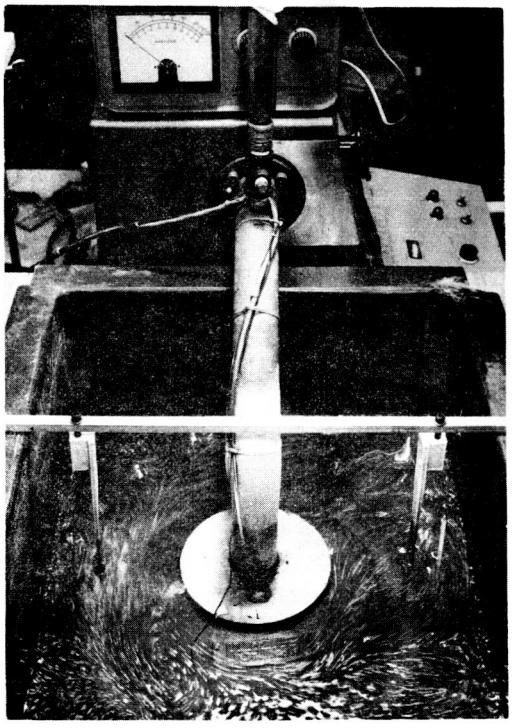
(a) SAMPLE



(b) SAMPLE SUSPENDED



(c) SPHERE OPEN



(d) SPHERE IMMERSED

FIGURE I-1 - VIEWS OF THERMAL EMITTANCE SAMPLE AND EQUIPMENT

microns of mercury, $k_1 = 1.26 \times 10^{-4}$ watts for the conditions here. A plot of W versus p with $(T_S - T_C)$ as parameter is shown in Figure I-2. The chamber temperature was measured by two copper constantan thermocouples. The chamber temperature (T_C) was maintained at 200°K or less by immersing the chamber in a bath of dry ice and isopropanol (see Figure I-1(d) for a view of the immersed sphere). The total hemispherical emittance was computed from the following equation:

$$P = \frac{\epsilon_S \, \epsilon_C \, \sigma \, A_S \, (T_S^4 - T_C^4)}{\epsilon_C + \frac{A_S}{A_C} \epsilon_S - \frac{A_S}{A_C} \epsilon_S \, \epsilon_C} + K \, (T_S - T_C) \qquad \text{Eq. 1}$$

where P = power applied to sample.
ϵ_S, ϵ_C = sample, chamber emittances
A_S, A_C = sample, chamber areas
T_S, T_C = sample, chamber temperatures
K = constant covering conduction losses

For the present case, it was shown that to within 0.04%, the equation reduced to

$$P = \epsilon_S \, A_S \, \sigma \, (T_S^4 - T_C^4) + K \, (T_S - T_C) \qquad \text{Eq. 2}$$

Re-arranged, this became

$$\epsilon_S \, A_S = \frac{P - K \, (T_S - T_C)}{\sigma \, (T_S^4 - T_C^4)} \qquad \text{Eq. 3}$$

Since the samples contained surfaces other than those for which the emittance is required, in calculations

$$\epsilon_S \, A_S = \epsilon_1 \, A_1 + \epsilon_2 \, A_2 + \cdots \qquad \text{Eq. 4}$$

The evaluation of the areas and emissivities for these other surfaces was extremely important. The edges of the solar cells contributed 10% to the total area of the cells. A separate emittance run with etched P-silicon blanks resulted in an emittance of 0.6 for these edges. Runs with brass blocks alone, and with a soldered block, gave emittance values of 0.08 and 0.11 respectively. For silver contacts, an emittance of 0.04 was assumed.

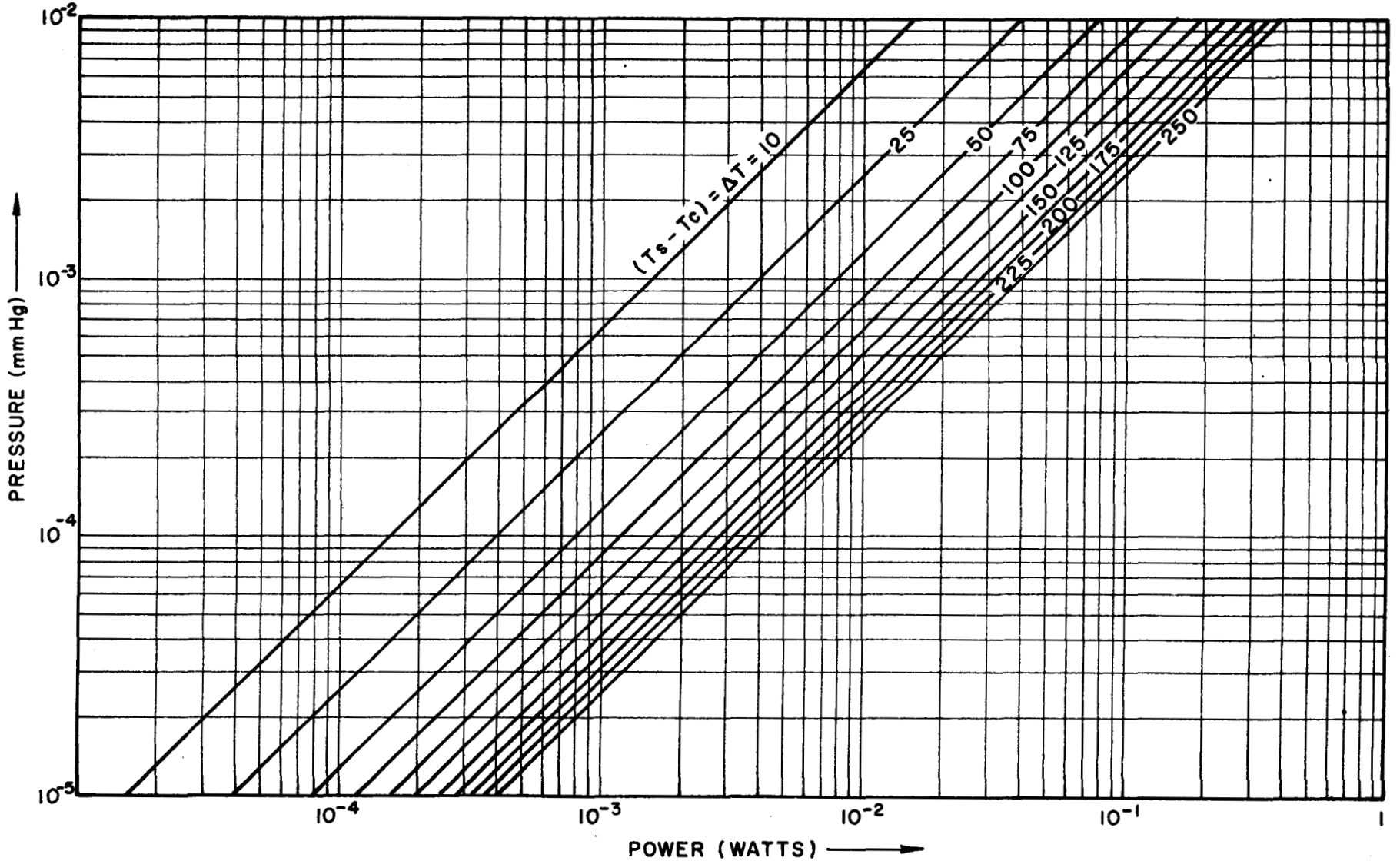


FIGURE I-2- POWER LOSS VS. PRESSURE AS A FUNCTION OF TEMPERATURE DIFFERENCE BETWEEN SAMPLE AND SURROUNDINGS

An identical resistor was connected in series with that heating the sample, and a measure of the power dissipated in this resistor, gave the sample power. Sample powers were measured to within ± 1%. Sample temperatures could be measured to ± 1°C, and the chamber temperatures to ± 1.5°C. This gave errors in the emittance values of 2.5% and 3.5% at sample temperatures of 400°K and 300°K respectively.

It was found that a long time elapsed before thermal equilibrium was reached. Since the temperature versus time curve was exponential, the following equation could be applied.

$$T_e = \frac{(T_2 - T_1)(T_3 - T_2)}{(T_2 - T_1) - (T_3 - T_2)} + T_2 \qquad \text{Eq. 5}$$

where T_1, T_2 and T_3 were temperatures taken at equal increments of time.

As an example of the calculation, the 58°C run on sample G is taken. Table I-1 shows the raw data. Column 1 was the pressure measured on an ionization gauge. Column 2 was the bath temperature observed on a liquid-in-glass thermometer. The voltages from thermocouples are shown for the sample (Column 3), and the chamber (Columns 4 and 5). The reference junction was an ice bath at 0°C. Column 6 shows the voltage drop across the resistor in series with the heater, and squaring this voltage, and dividing by the resistance gave the power. Column 7 shows the sample temperature, obtained by referring Column 3 to NBS thermocouple tables. Column 8 gives the time corresponding to the temperature reading of the sample. Column 9 shows the average thermocouple reading for the chamber.

Equilibrium temperature calculations obtained from equation 5 are shown in Table I-2. Finally the computation was completed as follows:

$$\begin{aligned} T_s &= 330.78\ ^\circ K \\ T_c &= 194.00\ ^\circ K \\ T_s - T_c &= 136.78\ ^\circ K \\ T_s^4 &= 119.72 \times 10^8\ (^\circ K)^4 \\ T_c^4 &= 14.16 \times 10^{18}\ (^\circ K)^4 \\ T_s^4 - T_c^4 &= 105.56 \times 10^8\ (^\circ K)^4 \end{aligned}$$

1 Pressure (torr)	2 Bath Temp. (°C)	3 Sample Thermo- couple (mV)	4 Chamber Thermo- couple 1 (mV)	5 Chamber Thermo- couple 2 (mV)	6 Voltage Across Sample (V)	7 Sample Temper- ature (°C)	8 Time After Start (min)	9 Average Chamber Thermo- couple (mV)
1.3×10^{-5}	-73.2	1.189	-2.731	-2.753	6.952	29.88	5	-2.742
1.3×10^{-5}	-73.2	1.448	-2.731	-2.754	6.950	36.12	10	-2.743
1.3×10^{-5}	-73.5	1.648	-2.731	-2.753	6.949	40.93	15	-2.742
1.3×10^{-5}	-73.6	1.813	-2.730	-2.753	6.945	44.81	20	-2.742
1.3×10^{-5}	-73.6	1.936	-2.729	-2.752	6.945	47.69	25	-2.741
1.3×10^{-5}	-73.7	2.031	-2.728	-2.751	6.953	49.91	30	-2.740
1.3×10^{-5}	-73.6	2.107	-2.726	-2.750	6.946	51.68	35	-2.738
1.3×10^{-5}	-73.6	2.163	-2.725	-2.749	6.958	52.98	40	-2.737
1.3×10^{-5}	-73.6	2.205	-2.723	-2.748	6.932	53.95	45	-2.736
1.3×10^{-5}	-73.6	2.238	-2.722	-2.747	6.958	54.72	50	-2.735
1.3×10^{-5}	-73.4	2.264	-2.720	-2.745	6.949	55.33	55	-2.733
1.3×10^{-5}	-73.4	2.283	-2.718	-2.743	6.956	55.77	60	-2.731
1.3×10^{-5}	-73.4	2.299	-2.715	-2.741	6.961	56.14	65	-2.728

TABLE I-1. Raw Data For Emittance Measurements

T_1 (°C)	T_2 (°C)	T_3 (°C)	T_2-T_1	T_3-T_2	$(T_2-T_1)(T_3-T_2)$	$(T_2-T_1)-(T_3-T_2)$	$\frac{(T_2-T_1)(T_3-T_2)}{(T_2-T_1)-(T_3-T_2)}$	T_e (°C)
29.88	36.12	40.93	6.24	4.81	30.01	1.43	20.99	57.11
36.12	40.93	44.81	4.81	3.88	18.66	0.93	20.06	60.99
40.93	44.81	47.69	3.88	2.88	11.17	1.00	11.17	55.98
44.81	47.69	49.91	2.88	2.22	6.39	0.66	9.68	57.37
47.69	49.91	51.68	2.22	1.77	3.93	0.45	8.73	58.64
49.91	51.68	52.98	1.77	1.30	2.30	0.47	4.89	56.57
51.68	52.98	53.95	1.30	0.97	1.26	0.33	3.82	56.80
52.98	53.95	54.72	0.97	0.77	0.747	0.20	3.73	57.68
53.95	54.72	55.33	0.77	0.61	0.470	0.16	2.94	57.66
54.72	55.33	55.77	0.61	0.44	0.268	0.17	1.58	56.91
55.33	55.77	56.14	0.44	0.37	0.163	0.07	2.33	58.10

Average T_e = 57.62°C = 330.78°K.

TABLE I-2. Equilibrium Temperature for Emittance Measurements

$\sigma = 5.67 \times 10^{-12}$ watts/cm^2 (°K)^4

$\sigma(T_s^4 - T_c^4) = .0598$

Conduction losses = $K (T_s - T_c) = .002$ watts

Power dissipated $= \frac{(6.95)^2}{100} = 0.483$ watts

$\therefore$ net power radiated = 0.481 watts

Correction ($A\epsilon$) product = 0.722

Using equations 3 and 4:

$$\epsilon_s \cdot A + (\text{correction } \epsilon A \text{ products}) = \frac{\text{net power radiated}}{\sigma (T_s^4 - T_c^4)}$$

ie. $\epsilon_s \cdot A = \frac{0.481}{.0598} - .722 = 7.31$

$A = 7.7$ cm^2

$\therefore \epsilon_s = \frac{7.31}{7.7} = 0.95$

This straightforward, relatively tedious procedure was followed for each sample for 3 or 4 equilibrium temperatures. These results are summarized in Figures 13, 14 and 15.